

UNCLASSIFIED

| |
|--|
| |
| |
| |
| AD NUMBER |
| ADC950035 |
| NEW LIMITATION CHANGE |
| TO Approved for public release, distribution unlimited |
| FROM Distribution: Further dissemination only as directed by Defense Threat Reduction Agency, 8725 John J. Kingman Road, Fort Belvoir, VA 22060-6201, 26 NOV 1974, or higher DoD authority. |
| AUTHORITY |
| DTRA ltr dtd 12 May 2009 |

THIS PAGE IS UNCLASSIFIED

UNCLASSIFIED



AD NUMBER

C950 035

CLASSIFICATION CHANGES

TO

UNCLASSIFIED

FROM

SECRET

AUTHORITY

31 DEC 89, IAW OCA MRKNGS ON DOCUMENT

THIS PAGE IS UNCLASSIFIED

UNANNOUNCED

SECRET

DNA 3396F

**OPERATION DIAL FLOWER
ANALYSIS OF
HIGH RESOLUTION OPTICAL DATA (U)**

ADC950035

Technology International Corporation
75 Wiggins Avenue
Bedford, Massachusetts 01730

26 November 1974

Final Report for Period 1 November 1972 - 31 December 1973

CONTRACT No. DNA 001-73-C-0116

THIS WORK SPONSORED BY THE DEFENSE NUCLEAR AGENCY
UNDER SUBTASK K47AAXYX948-03.

NOT TO BE ANNOUNCED IN DDC TAB

This document is not to be announced,
abstracted or cited in any announcement
media, secondary publication or general
bibliographic listing.

DDC
RECEIVED
FEB 11 1975
RECEIVED
E

50396

Prepared for

Director

DEFENSE NUCLEAR AGENCY

Washington, D. C. 20305

THIS DOCUMENT CONSISTS OF 116 PAGES,

COPY 1 OF 26 COPIES, SERIES A.

NATIONAL SECURITY INFORMATION

Unauthorized disclosure subject to
criminal sanctions.

CLASSIFIED BY: DD Form 254, 9 February 1973.
Contract No. DNA 001-73-C-0116. Exempt from
General Declassification Schedule of Executive
Order 11652. Exemption Category 3.
DECLASSIFY ON: 31 December 1989.

SECRET

When this report is no longer needed, Department of Defense Organizations will destroy it in accordance with appropriate procedures. Contractors will destroy the report according to the requirements of the Industrial Security Manual for safeguarding classified information.

Retention of this document by DoD Contractors is authorized in accordance with Paragraph 2, Industrial Security Letter 71L-3, dated 17 May 1971.



SECRET

SECRET

SECURITY CLASSIFICATION OF THIS PAGE (When Data Entered)

| REPORT DOCUMENTATION PAGE | | READ INSTRUCTIONS BEFORE COMPLETING FORM |
|--|-----------------------|--|
| 1. REPORT NUMBER DNA 3396 F | 2. GOVT ACCESSION NO. | 3. RECIPIENT'S CATALOG NUMBER |
| 4. TITLE (and Subtitle) OPERATION DIAL FLOWER ANALYSIS OF HIGH RESOLUTION OPTICAL DATA (U) | | 5. TYPE OF REPORT & PERIOD COVERED Final Report for Period 1 Nov 72-31 Dec 73 |
| | | 6. PERFORMING ORG. REPORT NUMBER 760 |
| 7. AUTHOR(s) Robert W. Deuel Keith B. Ronnholm Dennis E. Overbye | | 8. CONTRACT OR GRANT NUMBER(s) DNA 001-73-C-0116 |
| 9. PERFORMING ORGANIZATION NAME AND ADDRESS Technology International Corporation 75 Wiggins Avenue Bedford, Massachusetts 01730 | | 10. PROGRAM ELEMENT, PROJECT, TASK AREA & WORK UNIT NUMBERS NWET Subtask K47AAXYX948-03 |
| 11. CONTROLLING OFFICE NAME AND ADDRESS Director Defense Nuclear Agency Washington, D. C. 20305 | | 12. REPORT DATE 26 November 1974 |
| | | 13. NUMBER OF PAGES 116 |
| 14. MONITORING AGENCY NAME & ADDRESS (if different from Controlling Office) | | 15. SECURITY CLASS (of this report) SECRET |
| | | 15a. DECLASSIFICATION/DOWNGRADING SCHEDULE XGDS (89) |
| 16. DISTRIBUTION STATEMENT (of this Report) | | |
| 17. DISTRIBUTION STATEMENT (of the abstract entered in Block 20, if different from Report) | | |
| 18. SUPPLEMENTARY NOTES (S) Sensitive methods were used to collect data discussed in this report. The sensitive aspects of the collection program are described in Dial Flower Classification Guide (10 May 1972). Readers are urged to be familiar with this guidance before further disseminating the existence or substance of the data contained in | | |
| 19. KEY WORDS (Continue on reverse side if necessary and identify by block number) Atmospheric Nuclear Tests Optical Measurements Fireball Development Nuclear Debris Clouds | | |
| 20. ABSTRACT (Continue on reverse side if necessary and identify by block number) (S) Photographic data from three nuclear events (Fr. 44, Fr. 45, Fr. 46) and a high explosive safety experiment was obtained during DNA Operation Dial Flower as a result of optical documentation provided for the primary radar clutter experiments. Photographic data describing the geometry and spatial extent for each event is presented as a function of time. In addition, the spatial development of the debris cloud, including rise and expansion rates, was measured directly from photographic records. The dimensions and duration of the luminous phase of each | | |

DD FORM 1 JAN 73 1473 EDITION OF 1 NOV 65 IS OBSOLETE

SECRET

SECURITY CLASSIFICATION OF THIS PAGE (When Data Entered)

50396

SECRET

SECRET

SECRET

SECURITY CLASSIFICATION OF THIS PAGE(When Data Entered)

18. SUPPLEMENTARY NOTES (Continued)

this report. Current guidance may be obtained from DNA/ISCM. This work was sponsored by the Defense Nuclear Agency under Subtask K47AAXYX948-03.

20. ABSTRACT (Continued)

event were measured and plotted. Analysis of radiometric data from Fr. 45 was performed to yield color and brightness temperatures of this event.

SECRET

SECURITY CLASSIFICATION OF THIS PAGE(When Data Entered)

SECRET

SECRET

TABLE OF CONTENTS

| | | Page |
|-------|--|------|
| 1.0 | INTRODUCTION - - - - - | 3 |
| 1.1 | Background - - - - - | 3 |
| 1.2 | Instrument Operation - - - - - | 4 |
| 2.0 | PHOTOGRAPHIC TIME HISTORY - - - | 10 |
| 2.1 | Event Fr 44 (S) - - - - - | 10 |
| 2.2 | Event Fr 45 (S) - - - - - | 14 |
| 2.3 | Event Fr 46 (S) - - - - - | 19 |
| 2.4 | High Explosive Safety Experiment - - - - - | 24 |
| 3.0 | RESULTS - SPATIAL DEVELOPMENT - | 26 |
| 3.1 | Data Reduction Technique - - - - - | 26 |
| 3.2 | Pre-Event Geometry - - - - - | 27 |
| 3.3 | Measured Rise and Expansion Rates - - - | 32 |
| 3.3.1 | Event Fr 44 (S) - - - - - | 32 |
| 3.3.2 | Event Fr 45 (S) - - - - - | 35 |
| 3.3.3 | Event Fr 46 (S) - - - - - | 35 |
| 3.4 | Shock-Induced Phenomenon - - - - - | 38 |
| 4.0 | RADIOMETRY - - - - - | 46 |
| 4.1 | Introduction - - - - - | 46 |
| 4.2 | Luminous Areas vs Time - - - - - | 46 |
| 4.3 | Constant Density Contours - - - - - | 55 |
| 4.4 | Temperature Determination - - - - - | 62 |
| 4.4.1 | Introduction - - - - - | 62 |
| 4.4.2 | Radiance Measurements - - - - - | 64 |
| 4.4.3 | Temperature Calculations - - - - - | 71 |
| 4.4.4 | Discussion - - - - - | 77 |

SECRET

TABLE OF CONTENTS (Continued)

| | Page |
|------------|--|
| References | 79 |
| Appendix A | Instrument Plan - - - - - 81 |
| Appendix B | Data Record Summary - - - - - 85 |
| Appendix C | Refractive Correction - - - - - 99 |
| Appendix D | Atmospheric Transmission - - - - - 107 |

SECRET

1.0 INTRODUCTION (U)

1.1 Background (U)

(S) During the summer of 1972, a series of atmospheric nuclear detonations were conducted in the South Pacific and were monitored as part of DNA Operation Dial Flower. Technology International Corporation was responsible for providing high resolution optical photographic and videographic measurements of the formation, development, and late-time history of the debris clouds resulting from these tests.

(S) The Operation Dial Flower optical measurements performed by TIC were designed to:

- a) Provide optical image data of the spatial structure of the debris cloud as a function of time for correlation with the primary radar clutter experiments (0 to 2 minutes).
- b) Provide data documenting air entrainment, debris-air contact, torus formation, and turbulence in nuclear debris clouds for correlation with current theoretical models (0 to 15 minutes).
- c) Provide optical records of the events from which luminosity, temperature, and spectral information may be obtained (0 to 20 seconds).

A variety of photographic and electro-optical instrumentation systems were deployed to gather the required information.

(S) Mururoa, a coral atoll in the Tuamotu Archipelago of the South Pacific was the site of the nuclear weapons tests. There were three nuclear events in this particular test series plus a fourth non-nuclear event -- a high explosive safety shot from a tower in the lagoon. The three nuclear detonations were near-surface airbursts. In each case, the device was suspended

SECRET

(S)
from a tri-finned balloon. The test series was conducted from 25 June 1972 through 31 July 1972. Optical observations were made during all four events. Table I summarizes the time, yield, nominal height of burst and related information concerning each event.

(S) DNA employed both aircraft and ship platforms for the monitoring and experimental programs. TIC's measurements, along with the primary radar experiments, were conducted from the USNS Wheeling, a Pacific Missile Range instrumentation ship. The ship's course was planned as a constant radius arc around the test site area. The positions at zero time are shown in Figure 1. Table 2 contains the exact location and range of the ship at event time along with the look angle, which is clockwise azimuth from north to the event as measured from the ship. The ship range varied from 16.3 nautical miles to 19.8 nautical miles during the four events.

1.2 instrumentation Operation (U)

(S) In order to achieve the objectives of the Dial Flower Program, TIC designed and operated four types of camera systems. Large format, (5" and 9 1/2" film size) long focal length cameras were used to obtain the high resolution necessary for spatial structure. Shorter focal lengths coupled with large formats gave good coverage of late time cloud morphology. Radiometric measurements and fireball documentation necessitated the use of faster framing rate cine systems (typically greater than 10 fps). These systems employ smaller formats (16, 35, and 70mm) and a corresponding reduction of image size or field of view. Also employed were video systems as pointing controls for the other systems and for real-time analysis of pointing errors and general phenomenology. The complete instrument plan is contained in Appendix Table A-I. These instrument systems were chosen to fully cover the wide range of dimensions involved as the fireball expands

SECRET

TABLE 1 (S). OPERATION DIAL FLOWER EVENT TABULATION (U)

| DATE/ TIME | EVENT NO. | YIELD* (kt) | APPROX. HOB(meters) | SITE | REMARKS |
|--|--------------|----------------|------------------------|-------|--|
| 25 June 1972 1900 Z (1000 local) | Fr 44 | .4 ± .1 | 220 | North | Clear weather. Good view, 0 to 3 min. Later obscured by stratus cloud deck to H + 30 min. when some debris is visible as horizontal strata. |
| 30 June 1972 1830 Z (0930 local) | Fr 45 | 3.5 ± .5 | 210 | West | Good early, late time view. Obscured from 13 sec. to 2 min. |
| 27 July 1972 1840 Z (0940 local) | Fr 46 | 6.5 ± 1.5 | 215 | West | Fair early view. Scattered showers with 60-80% cloud cover. Fireball into clouds @ H + 2 sec., visible to 5 sec. Good late time view. |
| 31 July 1972 2230 Z (1330 local) | H E | Not Known | Tower | | One point detonation test. Cloud visible from H + 5 sec. to dispersion at H + 20 min. |

5

SECRET

Sec Ref. 1

SECRET

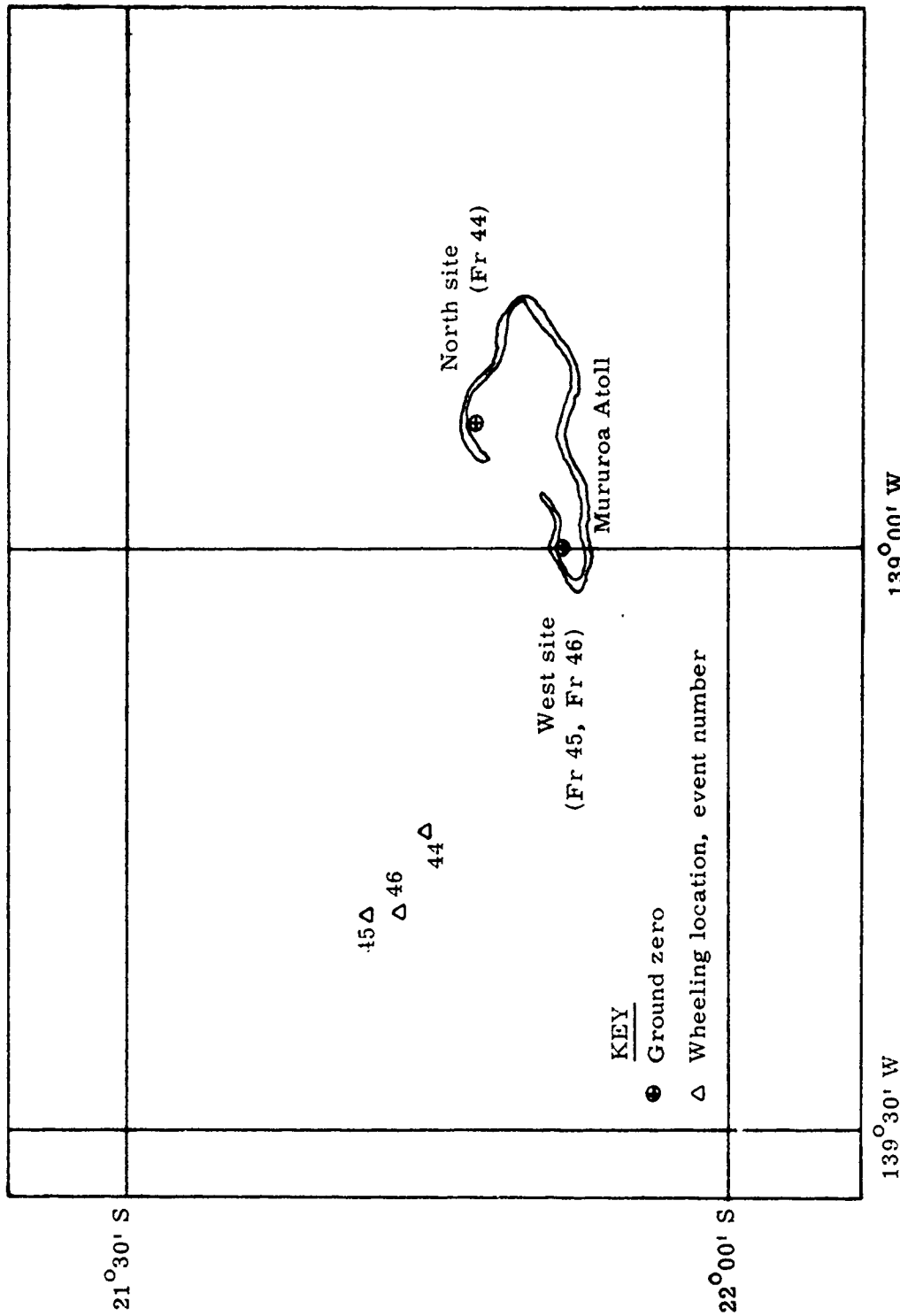


Figure 1 (S). USNS Wheeling location at detonation time (C).

SECRET

SECRET

TABLE 2 (S). USNS WHEELING POSITION PARAMETERS AT DETONATION TIME. (C)

| EVENT | FR 44 | FR 45 | FR 46 | HE |
|-------------------------|------------|------------|------------|------------|
| DATE | 25 JUNE 72 | 30 JUNE 72 | 27 JULY 72 | 31 JULY 72 |
| RANGE, (NAUTICAL MILES) | 19.486 | 19.820 | 19.208 | 16.254 |
| RANGE. (METERS) | 36070 | 36706 | 35574 | 30111 |
| LATITU DE | 21.746° S | 21.697° S | 21.715° S | 21.710° S |
| LONGITUDE | 139.243° W | 139.315° W | 139.314° W | 139.186° W |
| LOOK ANGLE | 96.318° | 117.603° | 117.128° | 105.978° |

SECRET

SECRET

to a fully developed cloud, and to cover a large radiant dynamic range for possible detonation of large yield devices. (For detailed information pertaining to the operation, refer to TIC Technical Report 743, DNA 3072F.)

(S) The field operation was successful with system operation greater than 90% for Fr. 45 and Fr. 46 and 100% for Fr. 44 and the H. E. event. The major factor limiting data collection was natural cloud cover which obscured some portions of each nuclear event, though the fireball was essentially visible for all events. Figure 2 shows the times of visibility. The non-nuclear safety experiment on the other hand occurred in conditions of excellent visibility under a nearly cloudless sky. A summary of each data record and its length may be found in Appendix B. (It should be noted that the final two digits of the record number correspond to the position number of each camera as presented on the instrument plan.)

SECRET

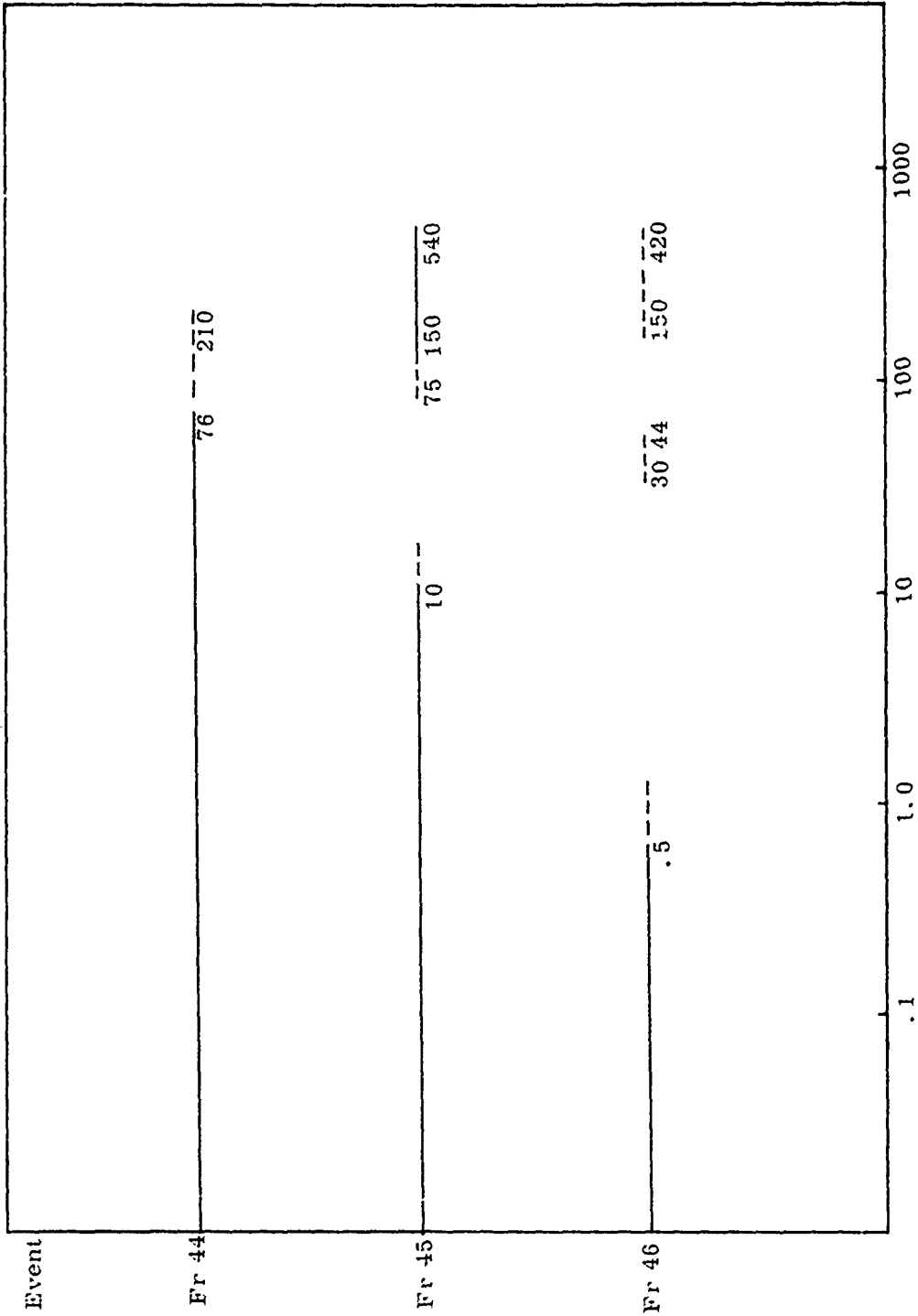


Figure 2 (S). Time duration of optical data acquired. Solid lines indicate good data; dashed lines indicate partial coverage; no lines indicate no significant data (U).

SECRET

SECRET

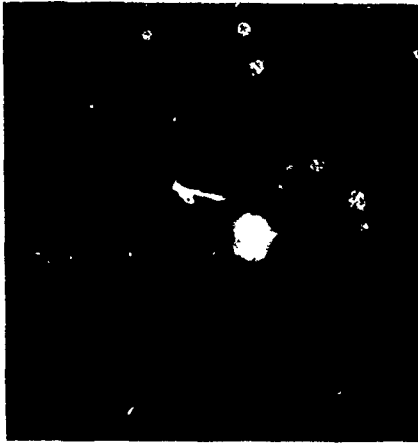
2.0 PHOTOGRAPHIC TIME HISTORY (U)

2.1 Event Fr 44 (S)

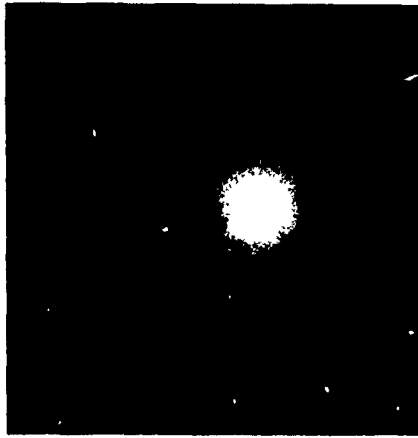
(S) The geometrical evolution of the first three seconds of Event Fr 44 are shown in Figure 3. The data frames shown were selected at 0.50 second intervals beginning 0.50 seconds after detonation from a black and white 35mm negative film exposed at 99.4 frames per second (record 61016). The apparent scattering of light in Figure 3 (a) and (b) is a photographic effect resulting from over exposure of the image and is not accurately representative of the source geometry at that time. Indications of a structure in the fireball beyond that of a simple sphere can be seen in (a), (b), and (c). The protuberances at the lower edge of the fireball are regions which are rendered visible by the excitation of the vaporized support cables. The structure of the fireball and the vaporized support cables may be viewed more clearly in Figure 4 (a) at .5 seconds. Traces of the support cables are still visible in 4 (b) and (c) which correspond to 3 and 5.5 seconds respectively.

(U) The photographs of Figures 4 and 5, reproduced at the same magnification, illustrate the rapid increase in diameter and altitude of the rising debris cloud. Figure 5 shows the continuing rise of the heated gases comprising the debris cloud from 44 to 55 seconds. Shortly after the (b) frame, the debris cloud began to be obscured by natural cloud cover. The entrainment of cold outside air into the turbulent cloud is suggested by the faint dark wisps at the lower right edge of the cloud. The pictures shown in Figures 4 and 5 were reproduced from a 9 1/2" color record.

SECRET



c) H + 1.51 sec



b) H + 1.01 sec

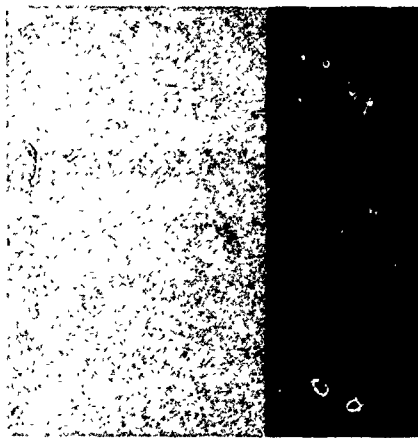
Scale:  = 300 m.



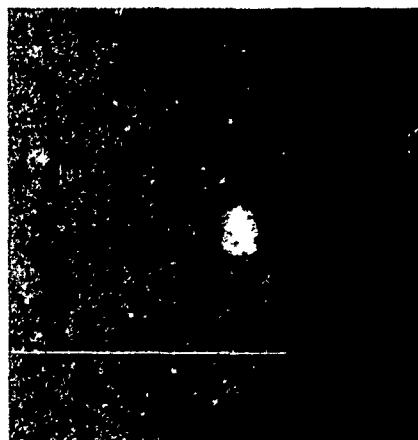
a) H + 0.50 sec



f) H + 3.02 sec



e) H + 2.52 sec



d) H + 2.01 sec

Figure 3 (S) Event Fr 44 - Fireball/Debris Cloud Luminous Phase (S) Record 61016;

SECRET

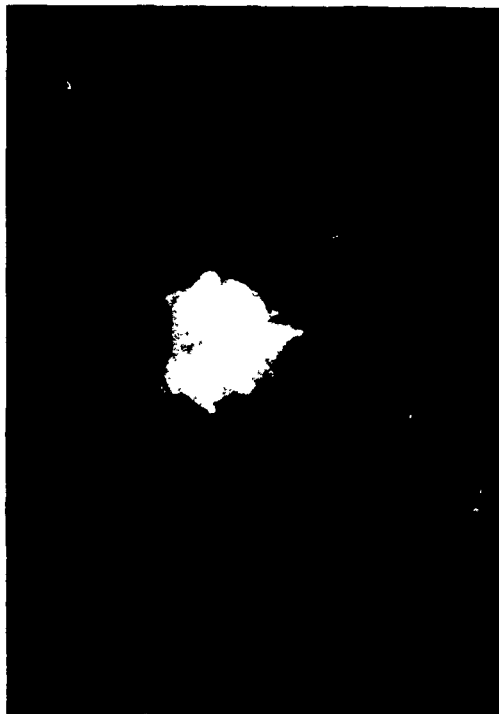
SECRET



b) H + 3.0 sec



d) H + 19.0 sec



a) H + 0.5 sec

Scale: $\text{L} = 100 \text{ m}$.

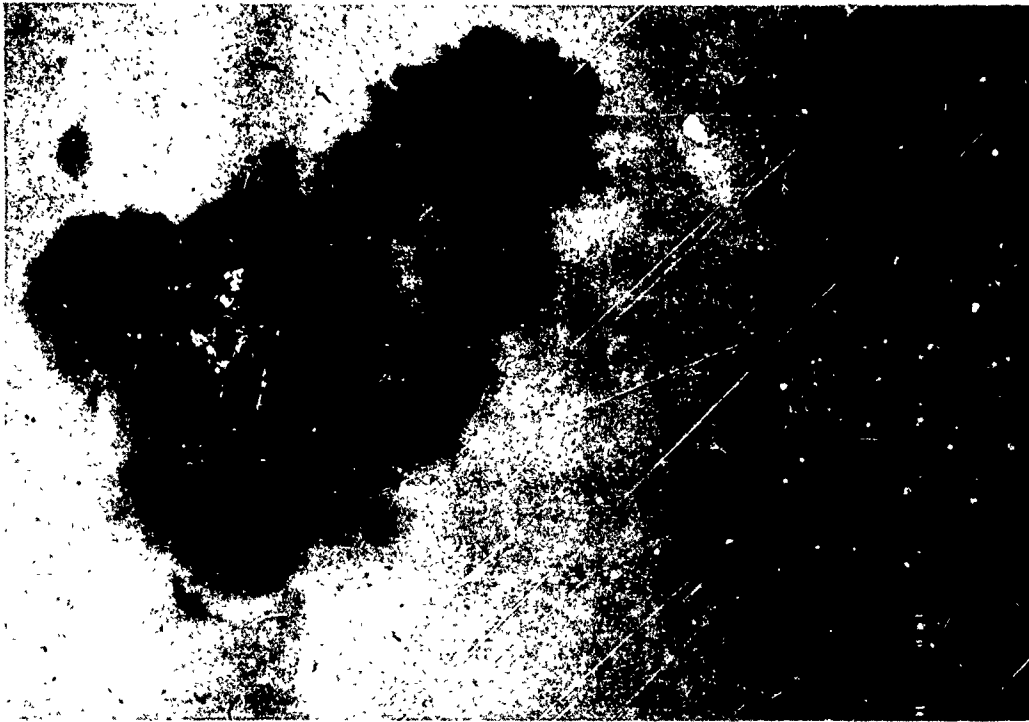


c) H + 5.5 sec

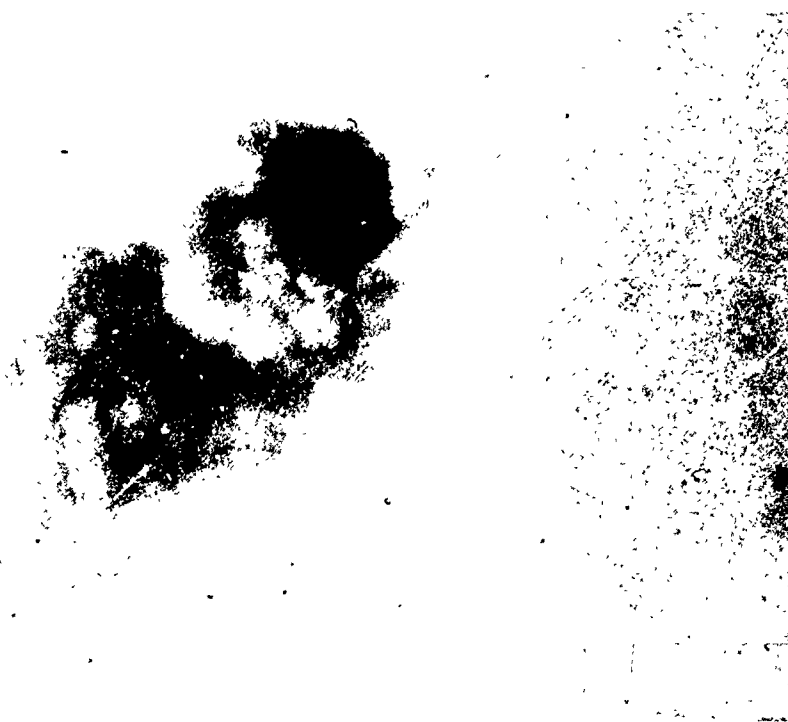
Figure 4 (S) Event Fr 44 - Debris Cloud Formation (S) Record 61025;

SECRET

SECRET



b) H + 55 seconds



a) H + 44 seconds Scale: $\text{---} = 100 \text{ m.}$

Figure 5 (S) Event Fr 44 - Late Time Debris Cloud Formation (S) Record 61025

SECRET

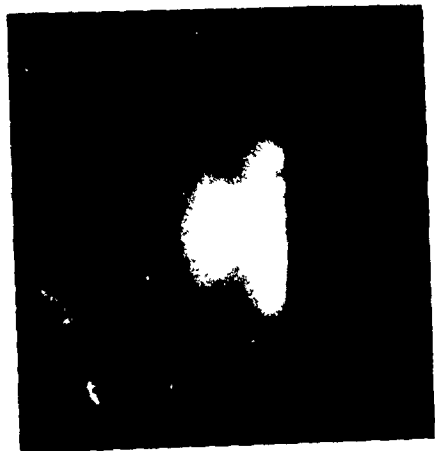
SECRET

2.2 Event Fr 45 (S)

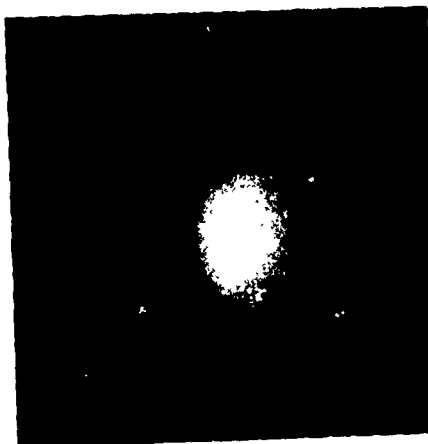
(S) Because of the larger yield (3.5 kt) of Event Fr 45, the fireball and debris cloud were luminous for almost twice the length of time as Event Fr 44, or for over six seconds. Figures 6 and 7 contain a sequence of pictures illustrating the development of the debris cloud from 0.48 seconds to 5.80 seconds at 0.48 second intervals. The condensation cloud can be seen building in Figure 6 (b) and (c) while its dispersion is evidenced as an increase in brightness and clarity in Figure 6 (d), (e), and (f). Also present is the linear movement of a shock associated disturbance which is visible as a small black feature on the horizon line to the right of center in Figure 6 (c) through (f). An axial asymmetry in the developing debris cloud is noticeable as a larger, brighter luminous area in the photographs comprising Figure 7. The effects manifested by the existence of this region are still noticeable at four minutes in Figure 9, (upper left hand portion of photograph) as a more developed cloud appearing at a greater altitude than the other portions. Figures 6 and 7 were selected from a 35mm black and white record filmed at 103.5 fps. The graininess of the pictures is due to the enlargement necessary for publication.

(S) The rise of the debris cloud into the overlying natural cloud bank is documented in Figure 8. These images were recorded with a long focal length lens on large format color film. Each photograph was recorded at 2.7 second intervals beginning at H + 3.6 seconds in this figure. Figure 8 (a) corresponds temporally to pictures (a) and (b) of the sequence of Figure 7 but is of a much higher resolution, showing significant additional structure. As in the prior event, Fr 44, the vaporized support cables are visible.

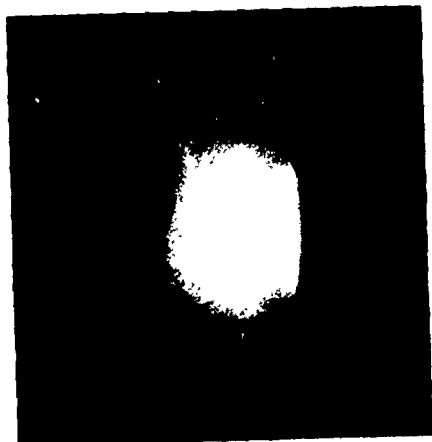
SECRET



c) H + 1.45 sec

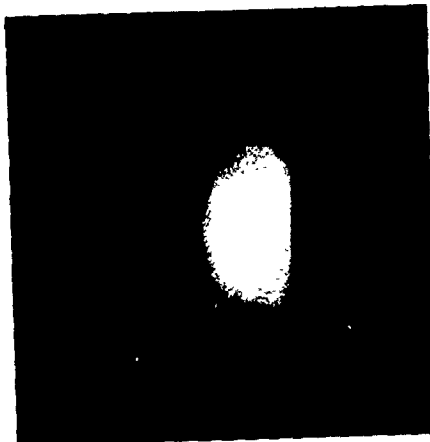


f) H + 2.90 sec

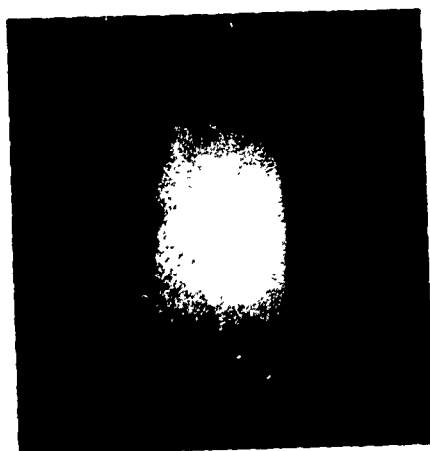


b) H + .97 sec

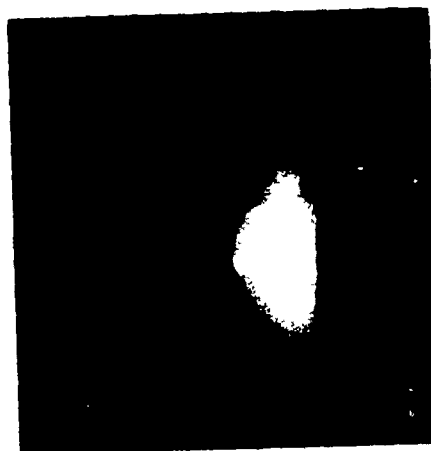
Scale:  = 300 m.



e) H + 2.42 sec



a) H + .48 sec

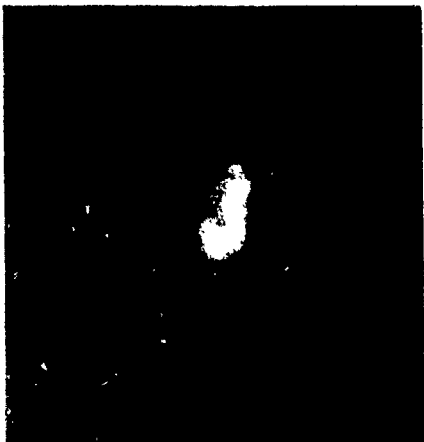


d) H + 1.93 sec

Figure 6 (S) Event Fr 45 - Fireball Luminous Phase (S) Record 61116

SECRET

SECRET



c) H + 4.35 sec



b) H + 3.86 sec



a) H + 3.38 sec

Scale: [] = 300 m.



f) H + 5.80 sec



e) H + 5.31 sec



d) H + 4.83 sec

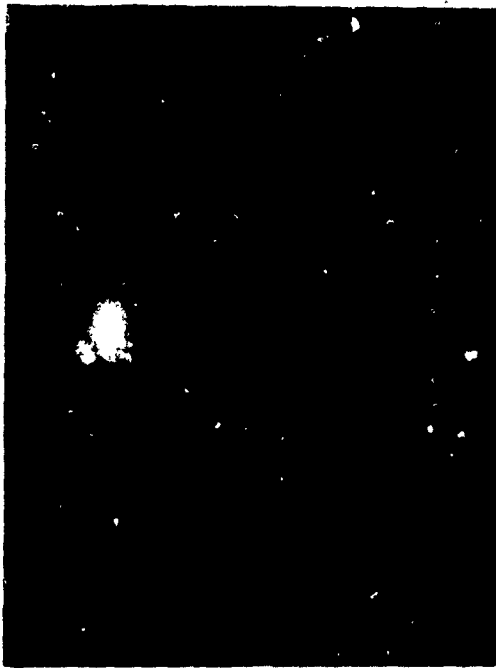
Figure 7 (S) Event Fr 45 - Fireball/Debris Cloud Luminous Phase (S) Record 61116

SECRET

SECRET



a) H + 3.6 sec Scale:  = 100 m. b) H + 6.3 sec



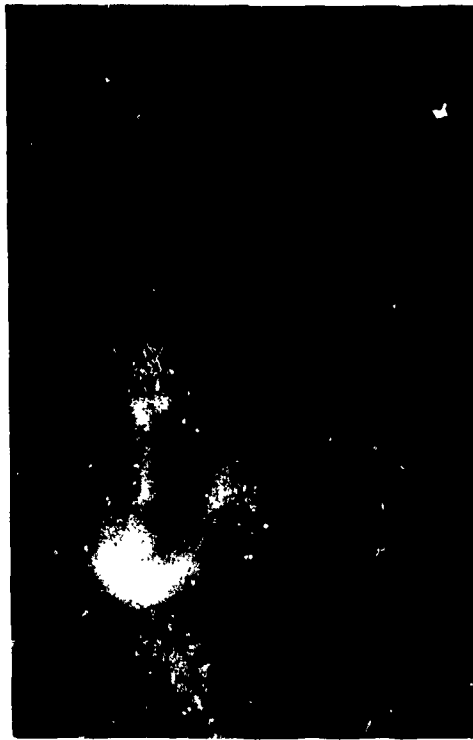
c) H + 9.0 sec d) H + 11.7 sec
Figure 8 (S) Event Fr 45 - Debris Cloud Formation (S) Record 61125

SECRET

SECRET



b) H + 3m 8 sec



d) H + 5m 13 sec



a) H + 1m 43 sec

Scale:  = 250 m.



c) H + 4m 18 sec

Figure 9 (S) Event Fr 45 - Late Time Debris Cloud (S) Record 61123

SECRET

SECRET

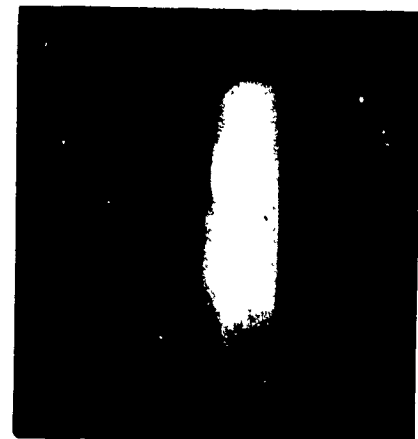
(C) At about 100 seconds after detonation the debris cloud again becomes visible from the Wheeling. Figure 9 shows the debris cloud from its emergence into view above the natural cloud layer until H + 5m13 sec. Clearly visible in the latter frame is a toroidal ring of debris. In the color original, this ring is an intense purple with reds and browns fading off to the sides.

2.3 Event Fr 46 (S)

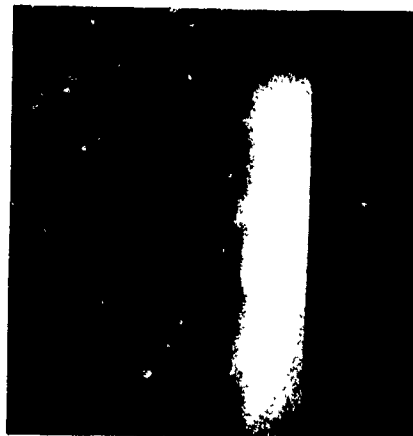
(S) For this event, the largest of the test series, the fireball and early development of the debris cloud were partially shielded from view by rain squalls in the area. Thus, the photographs of Figure 10 exhibit a lack of detail typically present. The time interval 0.5 to 3.0 seconds is shown at 0.5 second intervals. Each image has been enlarged from the 35mm original to the present size in which 1mm corresponds to 30 meters at ground zero. Frames (a) and (b) show the fireball rising into the layer of stratus and the initial development of the Wilson cloud. Only scattered light from rain droplets and Wilson cloud condensates is visible after 1.5 seconds, frames (c) - (f). The superstructure of a small French ship between the USNS Wheeling and the event is visible in the lower left of each frame.

(U) Undergoing expansion as it rises, the mushroom cloud again becomes visible after 32 seconds and remains visible for eight seconds before disappearing into another layer of clouds. The debris cloud appears to be reasonably symmetrical, and entrainment wisps can be seen at the lower edge of the cloud in Figure 11 (c) and (d).

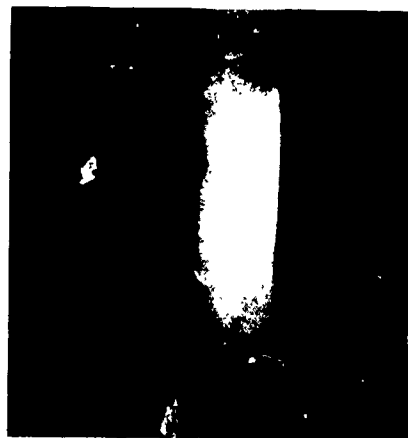
SECRET



c) H + 1.50 sec

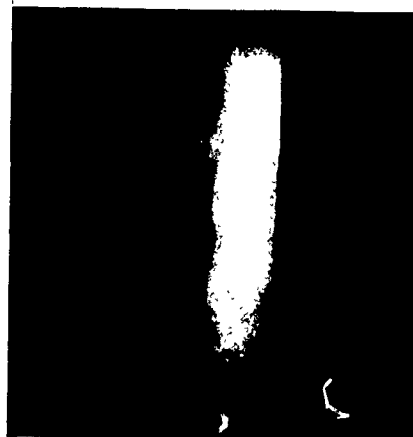


f) H + 3.00 sec

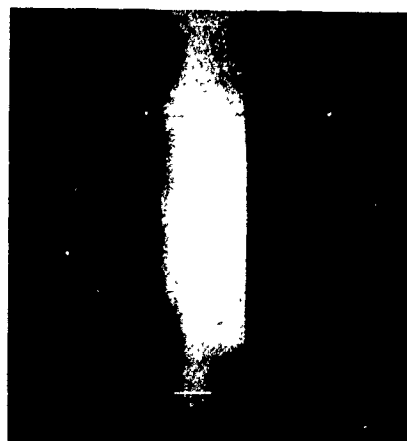


b) H + 1.00 sec

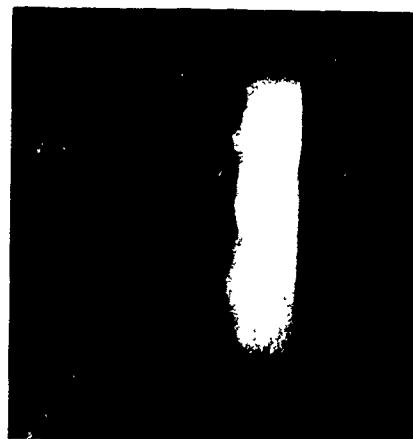
Scale:  = 300 m.



e) H + 2.50 sec



a) H + .50 sec

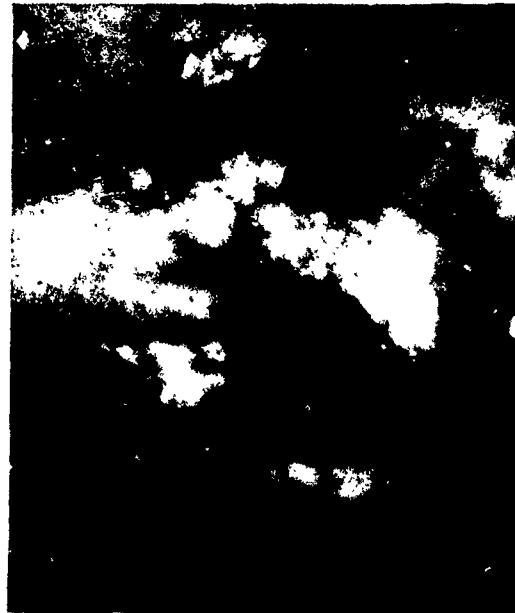
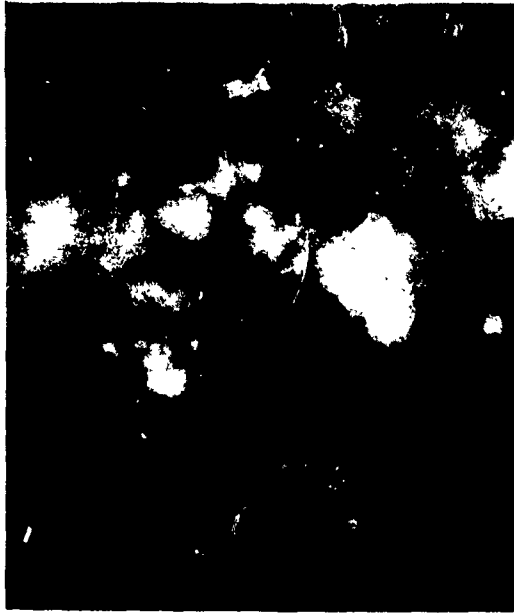


d) H + 2.00 sec

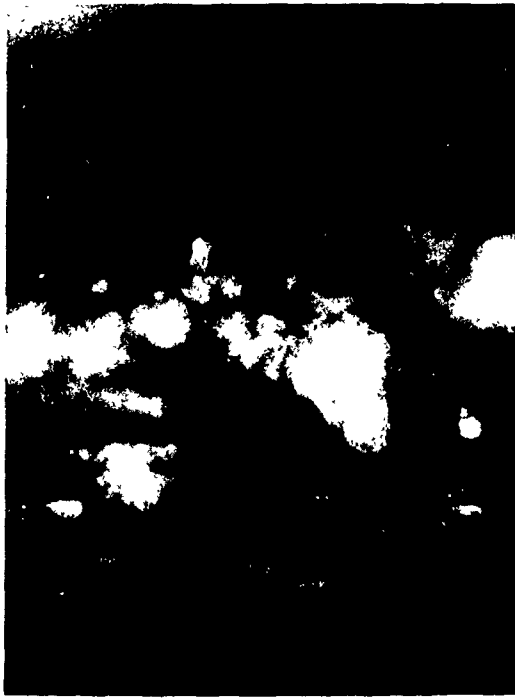
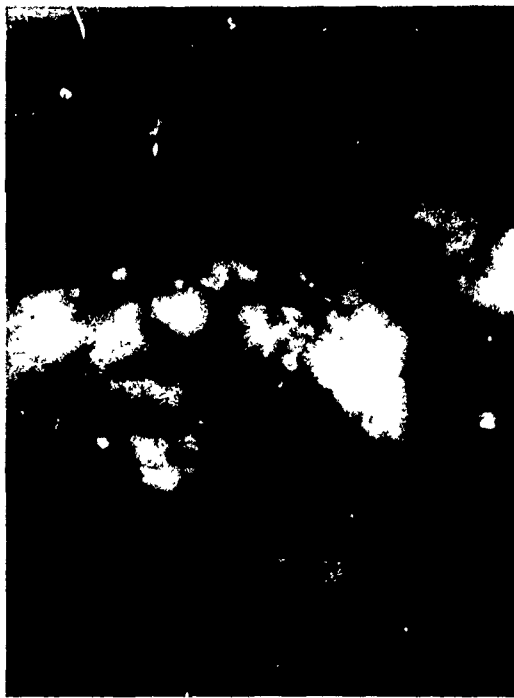
Figure 10 (S) Event Fr 46 - Fireball Luminous Phase (S) Record 61216

SECRET

SECRET



a) H + 32.5 sec Scale:  = 250 m. b) H + 35.0 sec



c) H + 37.5 sec

d) H + 40.0 sec

Figure 11 (S) Event Fr 46 - Debris Cloud Formation (S) Record 61124

SECRET

SECRET



b) H + 4m 36 sec



a) H + 3m 33 sec

Figure 12 (S) Event Fr. 46 - Late Time Debris Cloud (S) Record 61224; Scale:  = 250 m.

SECRET

SECRET



b) H + 6m 20 sec



a) H + 5m 38 sec

Figure 13 (S) Event Fr. 46 - Late Time Debris Cloud (S) Record 61224; Scale:  = 250 m.

SECRET

SECRET

(U) The debris cloud again becomes partially visible at 3m 30 sec., although it never completely emerges from behind intervening clouds. This sequence of high resolution cloud morphology photographs shown in Figures 12 and 13 extends for three minutes until 6m 20 sec. and shows the top of the cloud at an altitude of 6500 meters. The toroidal circulation of the debris cloud is clearly visible in Figures 12 (b) and 13 (c). Figures 11, 12, and 13 are comprised of photographs obtained originally on color film emulsion.

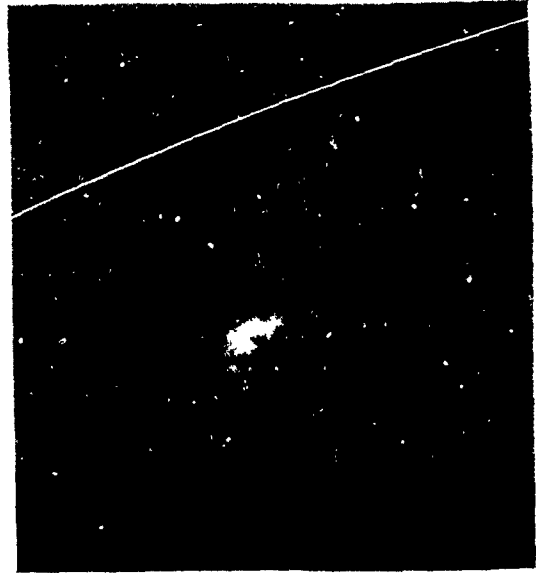
2.4 High Explosive Safety Experiment (U)

(S) The weather on 31 July, 1972, was the clearest for any of the tests during the summer and good optical data was obtained. Figure 14 contains four photographs illustrating the rise and expansion of the non-nuclear debris cloud. The cloud is visible due to reflected sunlight as the luminous phase was short lived. An apparent drift of the cloud top to the left in this figure indicates that winds may be present at the 500 meter level. The contrast difference between frames (a) and (b), and frames (c) and (d) is attributable to the use of different types of film for making the internegative necessary to produce black and white prints from a color positive film. A high contrast film was used for (c) and (d) in order to bring out the detail of the cloud but this also causes usually invisible imperfections and scratches on the original to become apparent.

SECRET



a) H + 10 sec



b) H + 21 sec



c) H + 53 sec



d) H + 1m 30 sec

Figure 14 (S) High Explosive Safety Experiment Cloud Development (U)
Record 61324; Scale:  = 10 meters.

SECRET

SECRET

3.0 RESULTS - SPATIAL DEVELOPMENT (U)

3.1 Data Reduction Technique (U)

(S) The spatial structure of the fireball/debris cloud as a function of time was derived from data acquired for all three nuclear events. Measurements were made from photographic records and scaled according to the relationship between focal length and range:

$$\text{Object size} = (\text{Image size}) \frac{(\text{Range to object})}{(\text{focal length of lens})}$$

The above equation is assumed correct for horizontal object dimensions but when vertical object measurements referenced to the horizon are to be made, corrections for atmospheric refraction (subtractive) and the earth's curvature (additive) must be included.

(U) As is well known, the curvature of the earth limits the distance at which near surface objects can be seen. Bowditch (Ref. 2) states that the range of the visible horizon (R) is dependent upon the height of the observer (h) through the following relation:

$$R = 1.144 (h)^{1/2}$$

for h in feet and R in nautical miles. Applying this equation twice, once for the height of the observer and once for the height of the object above its local sea level, it is found that 43 meters is the additive correction for a nominal ground range of 20 nautical miles. Thus to find the object altitude above sea level, one must add 43 meters to the horizon-object vertical separation distance as optically measured.

(U) Light rays passing through the nominal altitude density regimes of the atmosphere are bent by atmospheric refraction. This effect makes objects appear to an observer near the earth's surface to have an increased altitude. An analysis and computation of this refraction effect may be

SECRET

(U) found in Appendix C. Table 3 summarizes the results of this calculation by listing the correction that must be subtracted from the apparent altitude (as corrected for curvature of the earth) to correctly calculate height above sea level. The estimated error of the refractive correction is of the order of one meter and is due to the combined influence of the approximations used in the calculations and non-standard atmospheric conditions.

(U) Taking into consideration the path corrections discussed in the previous two paragraphs, the following equation results:

$$\text{Actual height above sea level} = \left(\text{Measured Image Height} \times \frac{(\text{Range})}{(\text{Focal Length})} \right) + \text{Earth's Curvature Correction} - \text{Refractive Correction}$$

The total error in height calculations is approximately ± 10 meters and results from limits on the accuracy of image measurements, the changing height of the camera above sea level due to the roll of the ship, and refractive correction errors.

3.2 Pre-Event Geometry (U)

(S) At the time of detonation, the nuclear device was supported by a balloon which TIC photographed before each event. Some examples of these photographs are shown in Figure 15. A drogue chute, which ensures a wind stabilized balloon orientation, is visible as a small white image to the right of the balloon in Figure 15 (b). The results of measurements on the center of the tri-finned barrage balloons are shown in Figure 16. The height of the balloon and of the detonation for each event is given in Table 4. Video color and infrared recordings complemented the photographic records used for these observations. Also shown in this table is the estimated height of burst as extrapolated from the rise rate graphs. The tabulated heights are in good agreement for all events.

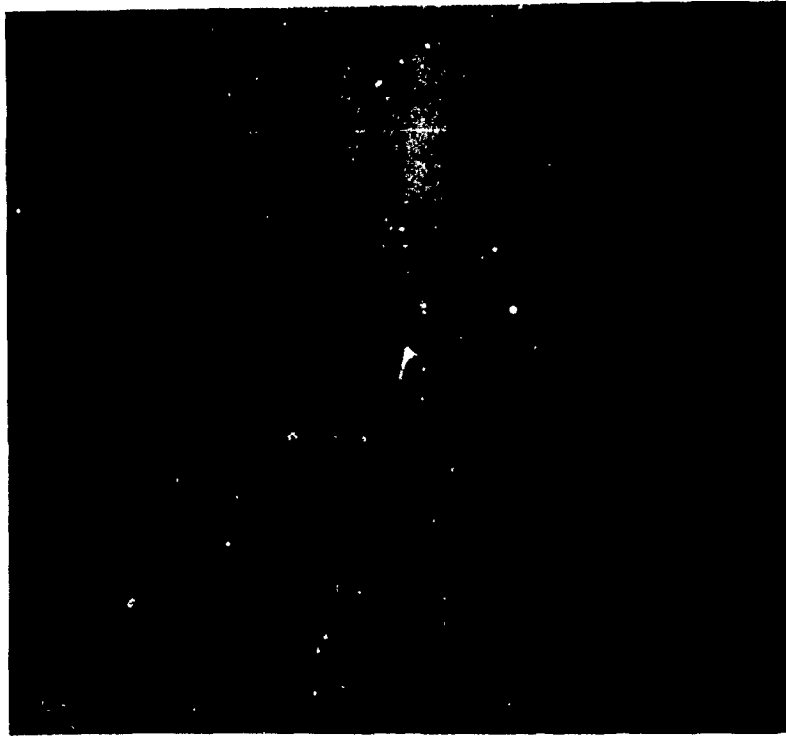
SECRET

TABLE 3. (U) REFRACTION CORRECTION (U)

| Apparent Altitude, (Meters) | Refractive Correction for 20 Nautical Mile Path, (Meters) |
|-----------------------------|---|
| 500 | 18.1 |
| 1000 | 17.5 |
| 2000 | 16.9 |
| 3000 | 16.2 |
| 4000 | 15.7 |
| 5000 | 15.1 |

Note: Estimated error in the correction is on the order of 1 meter or 5.5% at 500 meters due to approximations and actual atmospheric conditions

SECRET



b)



a)

Figure 15 (S) Pre-Event Suspension Balloon; (C) Documentary Record

Scale:  = 100 m.

SECRET

SECRET

| Perspective | Fr 44 | Fr 45 | Fr 46* |
|---------------------|-------|-------|--------|
| Event | | | |
| Diameter, meters | 28 | 22 | 29 |
| Length, meters | 51 | 56 | 70 |

Errors in these measurements are estimated to be $\pm 20\%$
Poor visibility

Figure 16 (S). Measured balloon dimensions (').

SECRET

SECRET

TABLE 4.(S) BALLOON AND DETONATION HEIGHTS (C)

| Event | Record | Balloon Center Height, (meters) | Detonation Height, (meters) | Balloon-device Separation, (meters) | Estimated Error, (meters) |
|-------|--------|---------------------------------|-----------------------------|-------------------------------------|---------------------------|
| Fr 44 | 61016 | 270 | 214 | 56 | ± 10 |
| | 61025 | 258 | - | - | ± 4 |
| | 61042 | 260 | 227 | 36 | ± 16 |
| | 61043 | - | - | - | ± 18 |
| Fr 45 | 61116 | - | 204 | - | ± 10 |
| | 61125 | 248 | - | - | ± 4 |
| | 61142 | 256 | 219 | 37 | ± 16 |
| | 61143 | 257 | 209 | 48 | ± 18 |
| Fr 46 | 61216 | - | 211 | - | ± 10 |
| | 61225 | 255 | - | - | ± 4 |
| | 61242 | 265 | 221 | 44 | ± 16 |
| | 61243 | 258 | 217 | 41 | ± 18 |

SECRET

(S) Another parameter of interest, the balloon-device separation, is tabulated in the last three columns of Table 4. The separation is calculated from the height of the balloon center and the height of the detonation, and varies from 33 to 56 meters. There appears to be no correlation of the balloon-device separation with yield.

3.3 Measured Rise and Expansion Rates (U)

3.3.1 Event Fr 44 (S)

(U) Good geometry data was obtained from zero to 76 seconds at which time the debris cloud became obscured by a natural cloud layer. Figure 17 presents the debris cloud height, width and vertical thickness measurements as determined from record #61022 (5 inch format) utilizing timing information from Record #61021 (70mm format). An expanded view of the early time portion of these measurements is shown in Figure 18. This latter data is derived mainly from infrared video recordings. If one extrapolates the line to zero time, a height of burst value of 225 meters results:

(S) Rise rates may be derived from the slope of the position versus time curve. The early rise rate of the fireball and torus is 20m/sec (averaged between 2-18 seconds) and decreases to the longer term cloud rise rate of 12/m sec (between 30-75 seconds). The horizontal and vertical expansion rates are 11 and 12 m/sec respectively at this time. These rates appear to be linear for the first 75 seconds, after which data is no longer available.

SECRET

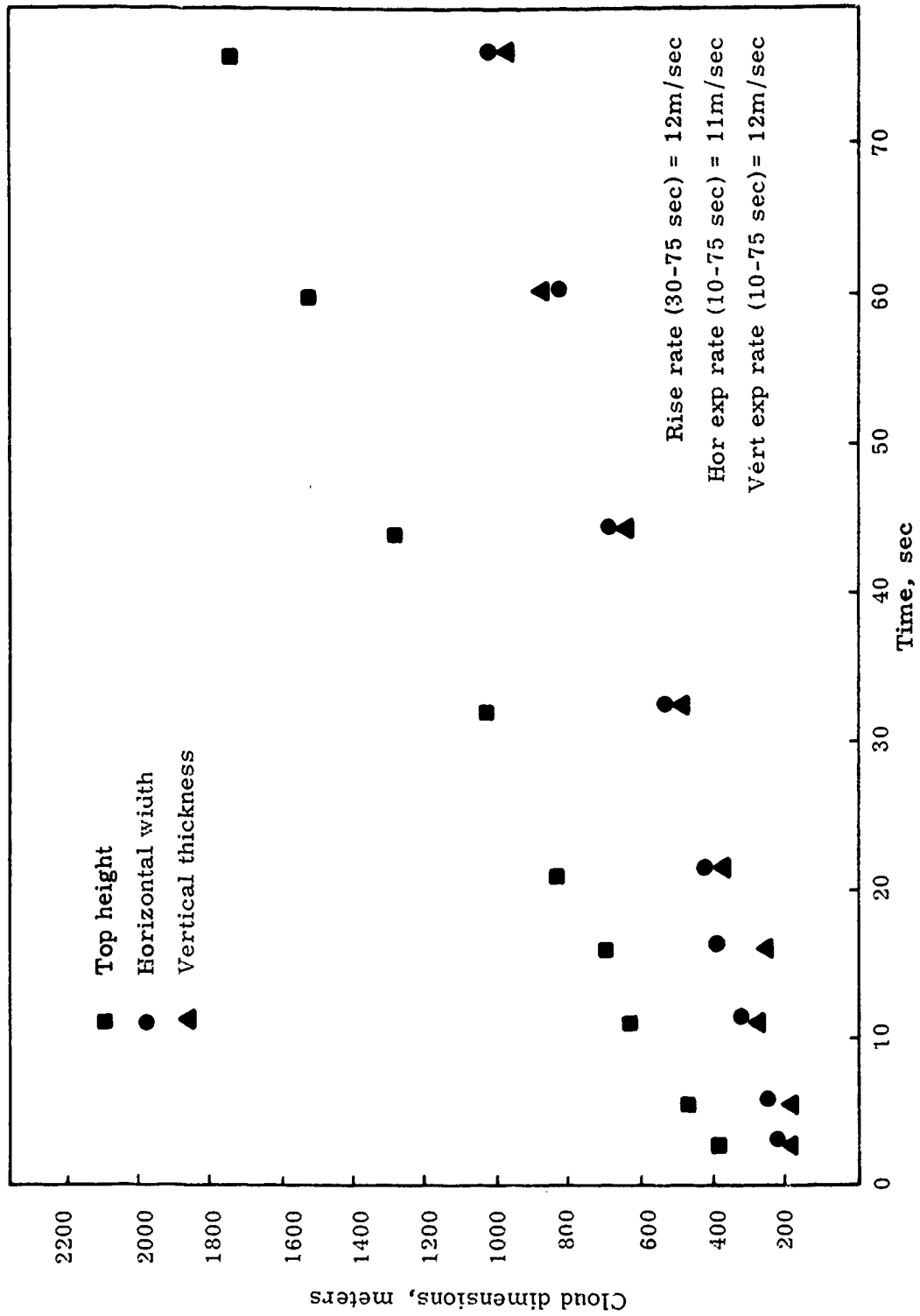


Figure 17 (S). Event Fr 44 - Cloud dimensional parameters vs. time. (S)

SECRET

SECRET

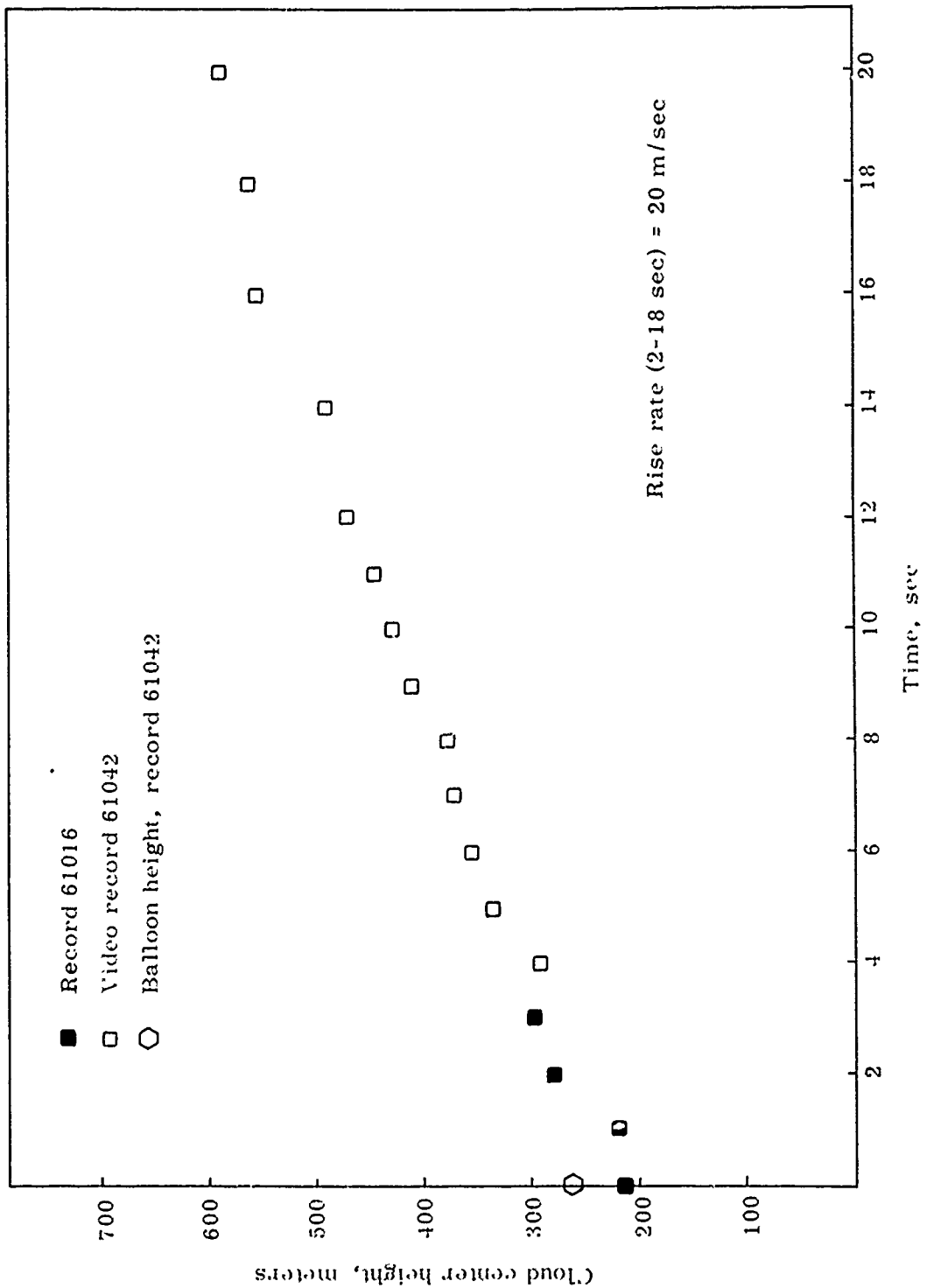


Figure 18 (S). Event Fr 44 - Early cloud height vs. time (debris cloud center). (S)

SECRET

SECRET

3.3.2 Event Fr 45 (S)

(S) After initial early time coverage, natural clouds obscured the rising source from 10 through 75 seconds. Positional data is presented in Figure 19 with Figure 20 showing the cloud center height at early times. The early time measurements were made mainly from color and infrared video tapes while the five inch format color records provided the late time data. From the height plot shown in Figure 20, the height of burst was extrapolated to be 200 meters.

(S) There are three rise rate time regimes which may be defined: the rise of the fireball and torus (1-10 seconds); the rapid rise of the cloud (1-100 seconds); and the slow upward drift of the cloud to its stabilization height. The rise rates (in m/sec) are:

| | <u>1-11 seconds</u> | <u>1-100 seconds</u> | <u>225-375 seconds</u> |
|--------|---------------------|----------------------|------------------------|
| Center | 37 | 23 | 1 |
| Top | -- | 25 | 3.3 |

Stabilization is reached at about four minutes at an altitude of 4.3 km. By comparison of Figure 18 and Figure 20 it can be seen that Event Fr 45 rises more rapidly than Event Fr 44 as one might predict because of the larger yield. The width and thickness could be measured for only 300 and 250 seconds with the expansion rates being 7.7 m/sec and 4.9 m/sec respectively.

3.3.3 Event Fr 46 (S)

(S) Data was obtained for three separate periods (0-1, 30-44, and 150-350 seconds) during the Fr 46 event due to the heavy cloud cover and intermittent rain squalls. Color and infrared video systems along with 35 and 70 mm film records provided the measurements for this event. The

SECRET

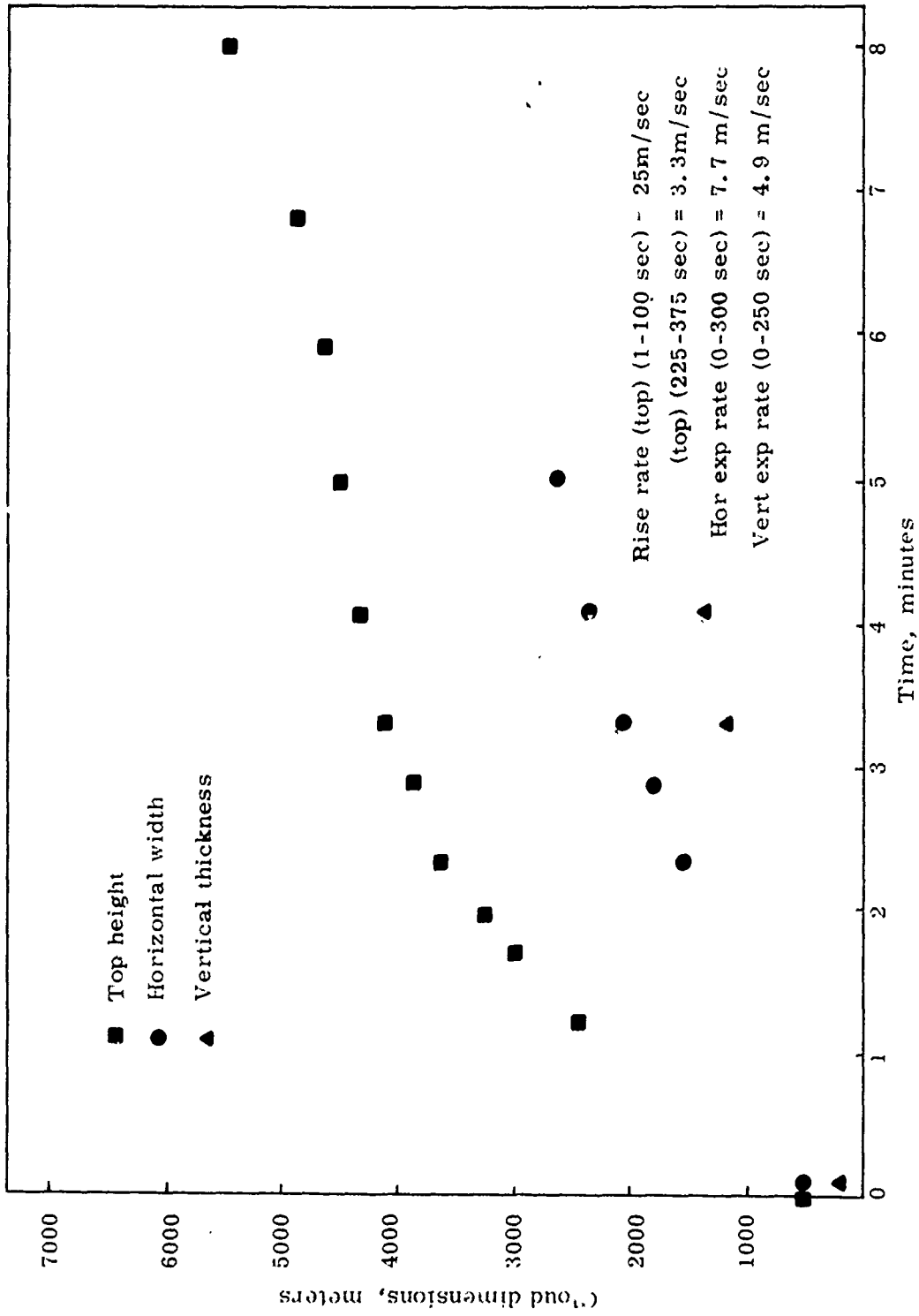


Figure 19 (S). Event Fr 45 - Cloud dimensional parameters vs. time. (S)

SECRET

SECRET

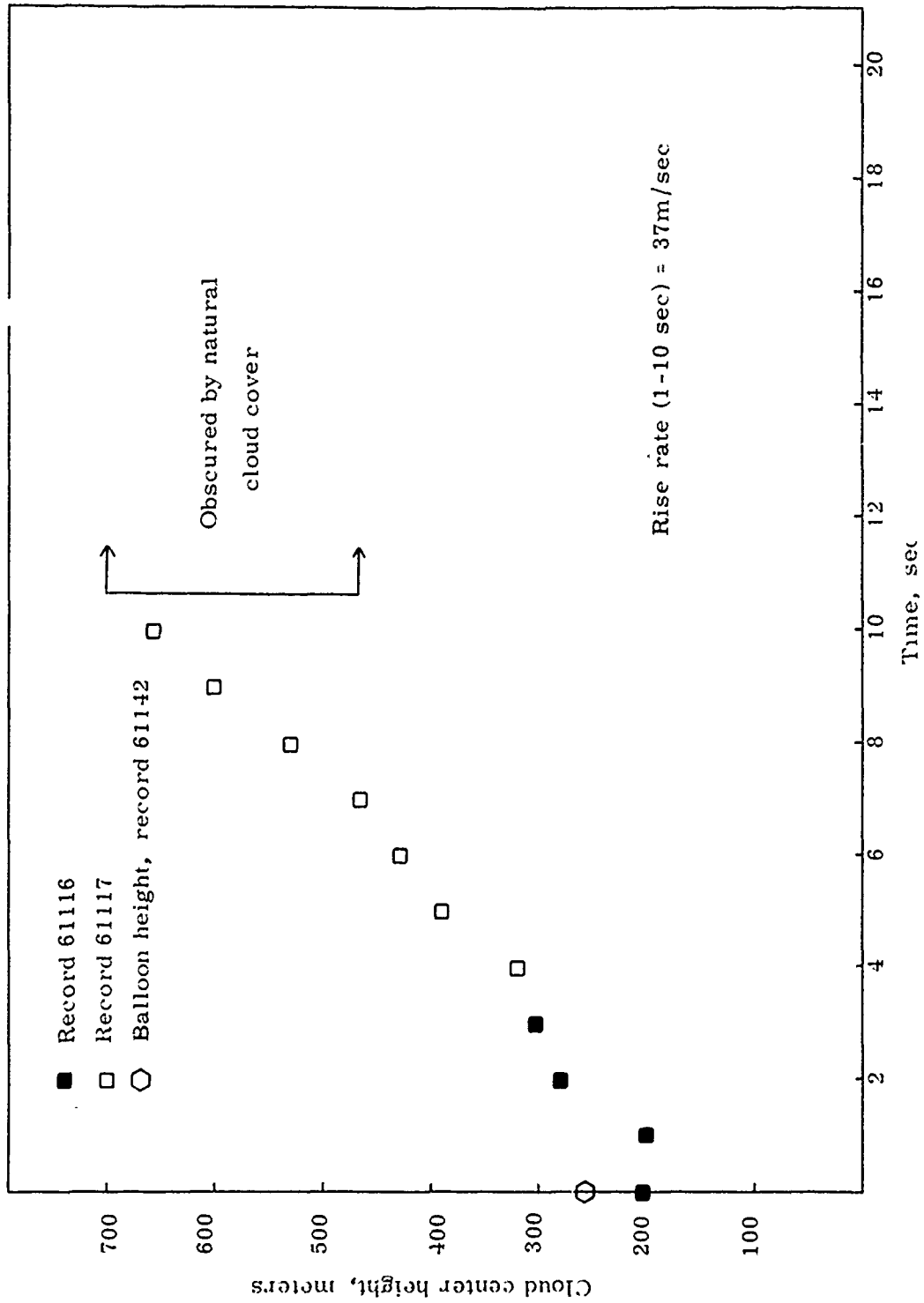


Figure 20 (S). Event Fr 45 - Early cloud height vs. time (debris cloud center). (S)

SECRET

SECRET

(S)

resulting spatial data is presented in Figure 21 and shows heights for the top and bottom of the cloud. The height of the fireball vs time is plotted in Figure 22 for the first second before it disappeared into the natural clouds.

(S) The rise rates calculated for this event are likely to be less accurate than those for the other events because of the scarcity of data points. The initial rise rate of the fireball thus determined is 135 m/sec (between .25 and 1.0 seconds) and decreases to 47 m/sec as the cloud develops (0-33 seconds). The final measurements of the rise rate for the top of the cloud give 12 m/sec (between 150-275 seconds). The horizontal and vertical expansion rates are 14 and 11 m/sec respectively for the 1-37 second time period.

3.4 Shock-Induced Phenomenon (U)

(S) A not unpredictable effect of a moderate sized detonation was observed during event Fr 45. An apparent shock-induced disturbance was observed moving away from ground zero along the sea surface as can be seen in Fig. 6. This effect would appear to be the physical motion of water and dust as a result of the outward moving blast wave. The position of the disturbance was measured for the 2.5 seconds it was visible and the result is plotted in Fig. 23. The apparent velocity of the disturbance, calculated from the slope of the curve, was found to be 290m/sec.

(S) In order to check the physical validity of this measured velocity, the theoretical shock wave velocity expected from a weapon of this yield was calculated. The governing equation (ref. 3) is:

$$U = c \left(1 + \frac{6\Delta P}{7P} \right)^{1/2}$$

where

U = shock wave velocity (m/sec)

c = speed of sound under ambient conditions (347 m/sec)

P = atmospheric pressure (14.7 psi)

SECRET

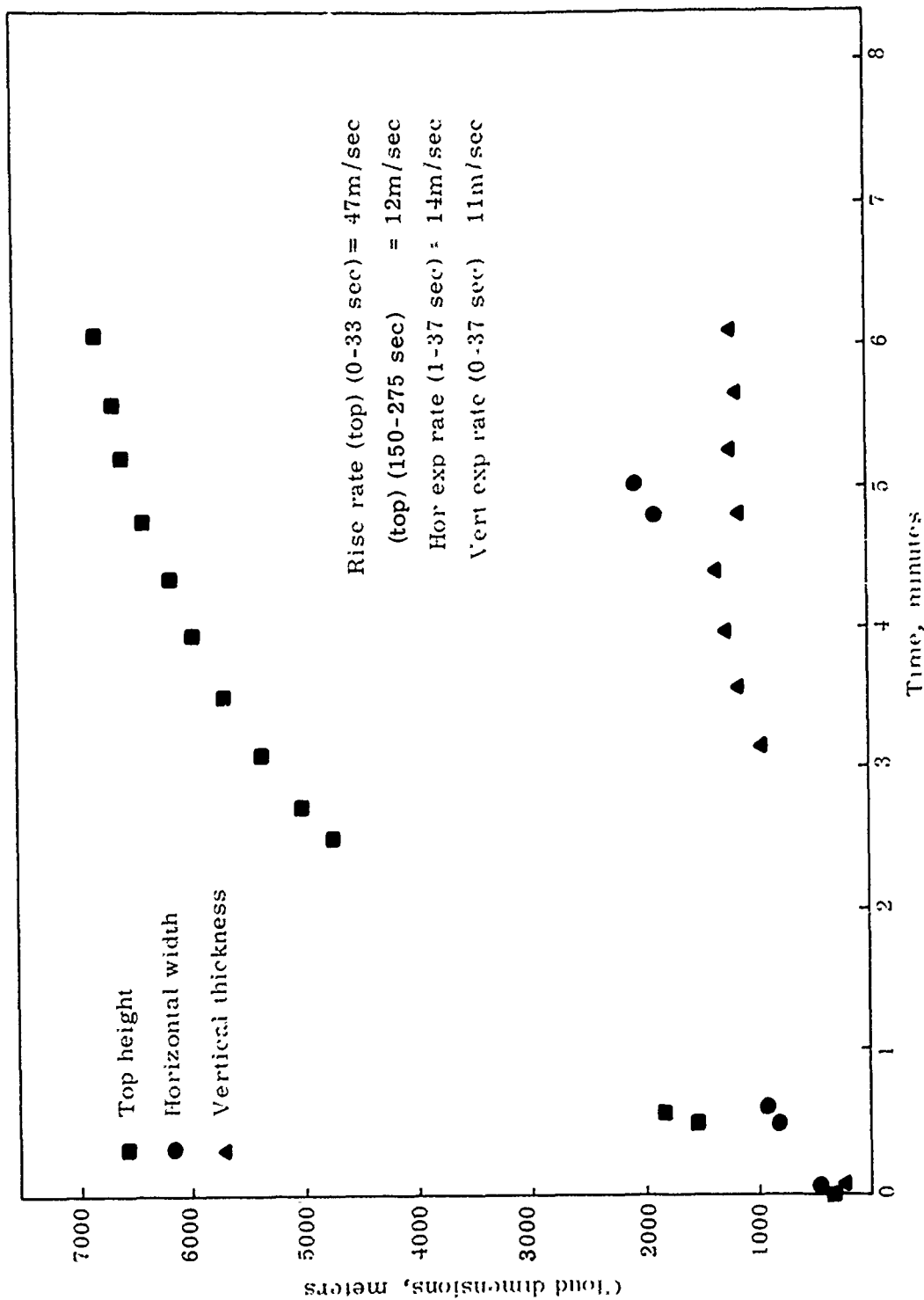


Figure 21 (S). Event Fr 46 - Cloud dimensional parameters vs. time. (S)

SECRET

SECRET

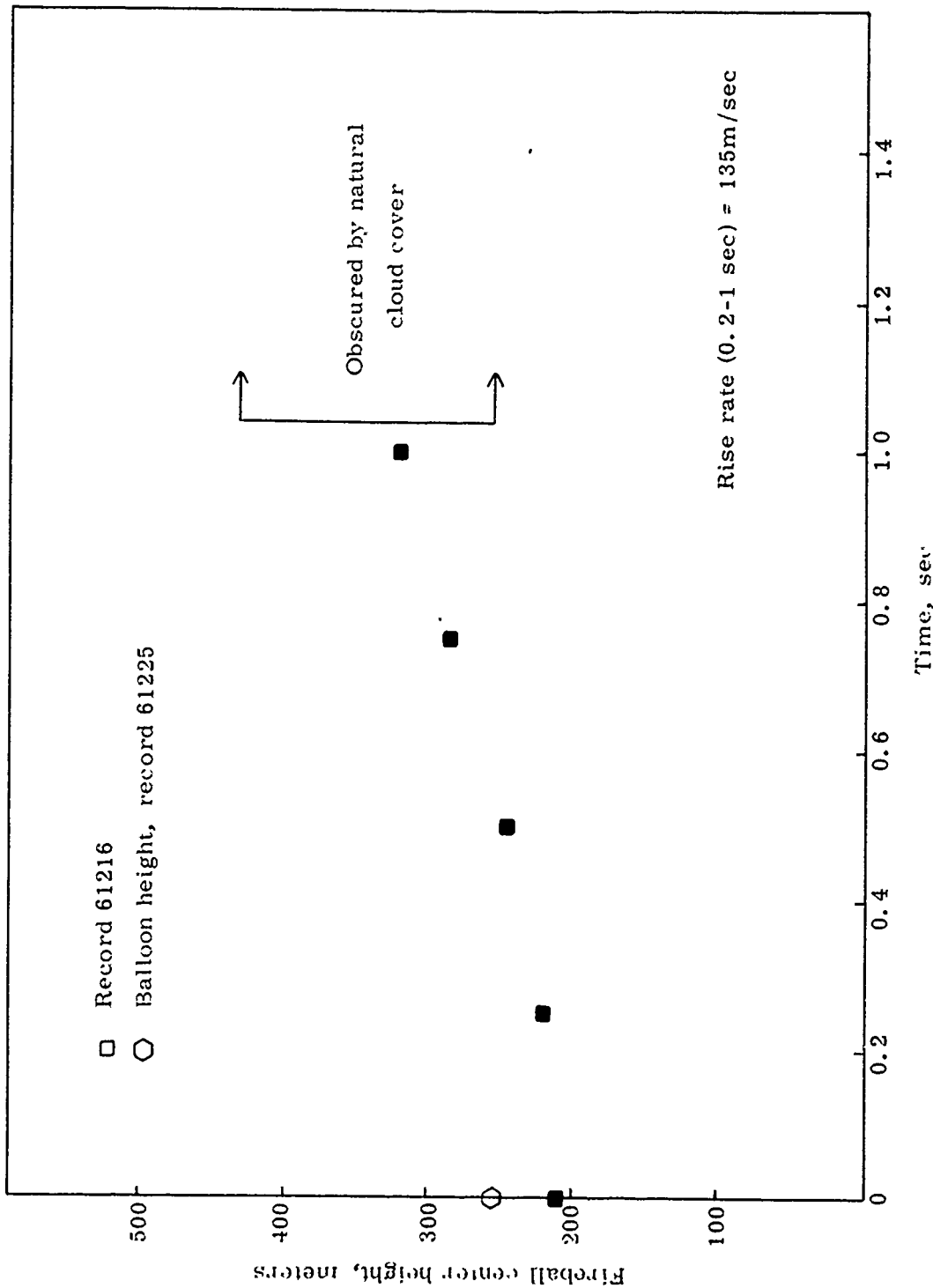


Figure 22 (S). Event Fr 46 - Fireball height vs. time. (S)

SECRET

SECRET

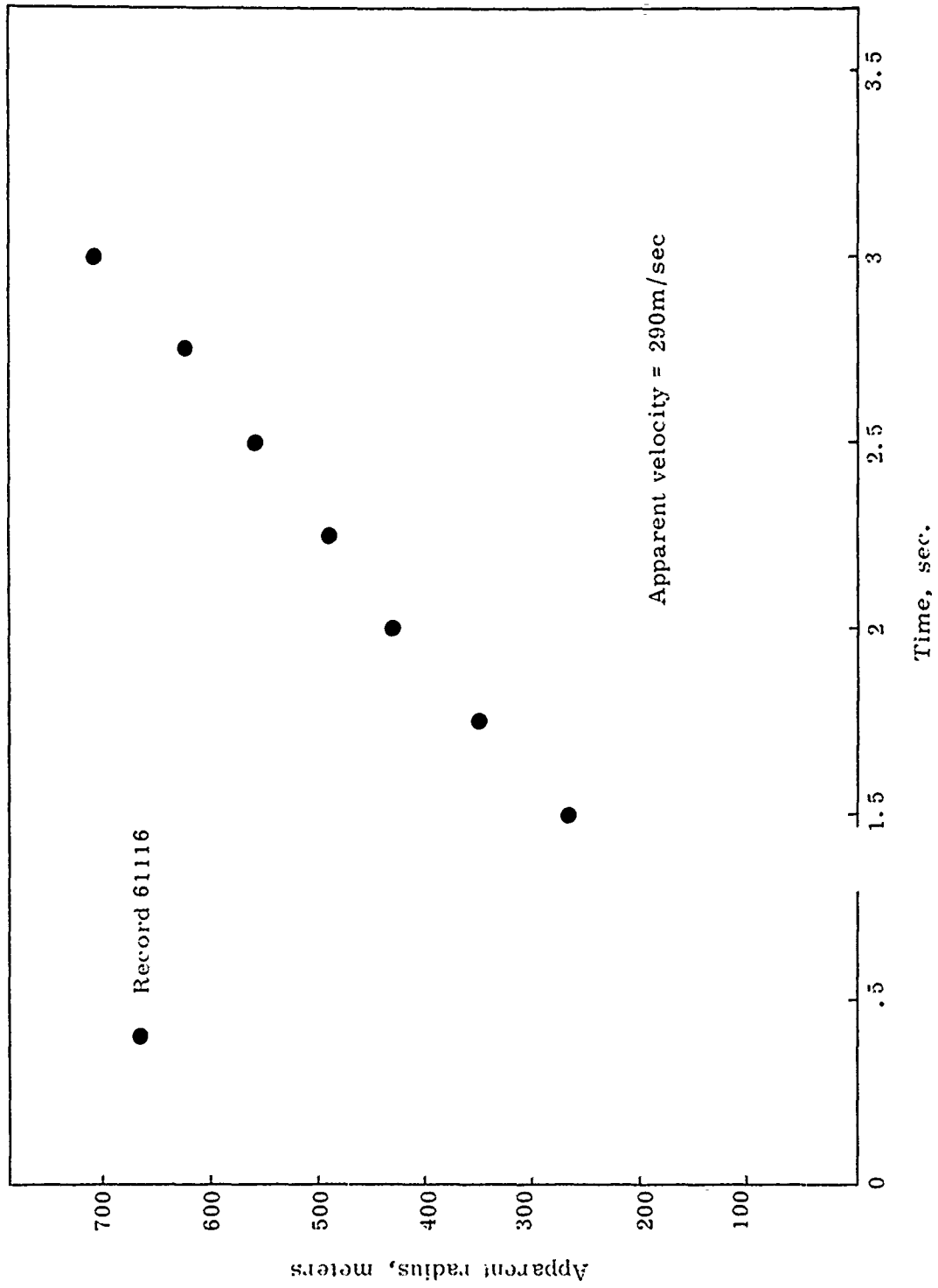


Figure 23 (S). Event Fr 45 - Shock associated surface disturbance radius vs. time (S).

SECRET

SECRET

(S) ΔP = overpressure due to blast wave (psi)

The value of the overpressure P can be calculated from the yield-normalized scaling laws,

$$x_1 = \left(\frac{W_0}{W}\right)^{1/3} \qquad y_1 = \left(\frac{W_0}{W}\right)^{1/3}$$

where x = measured distance from ground zero
 x_1 = scaled distance for 1 kT yield
 W = yield in kT
 W_0 = 1 kT yield
 y = measured height of burst
 y_1 = scaled height for a 1 kT detonation.

Overpressure is then determined as a function of the height of burst and range from reference data (Ref. 3).

(S) The scaled radius, overpressure, and the calculated shock propagation velocity are presented in Table 5. The calculated shock wave velocity U decreased from 575 to 420 m/sec as the distance from ground zero increases but remains greater than the optically measured apparent velocity of 290 m/sec.

(U) The discrepancy between calculated and measured values may result from a combination of two factors. First, the photographed physical disturbance may travel more slowly than the causal shock wave and secondly, the geometry of the situation is probably such that the measured velocity is a compressed projection of the true velocity onto the film plane.

(U) The former explanation depends upon the mechanism through which the surface is disturbed, and the nature of the surface materials present. However, for the following discussion in which a geometrical explanation is sought, the disturbance is assumed to have effectively the velocity of the shock wave. As the shock wave expands spherically, it intersects the sea surface plane.

SECRET

TABLE 5. (S) SHOCK ASSOCIATED DISTURBANCE PARAMETERS (U)

| Time (sec) | Radius, x (meters) | Scaled Radius, x_1 (meters) | Overpressure, ΔP (psi) | Shock Velocity, U (m/sec) | V_x calc (m/sec) | Angle, α (degrees) |
|---------------|-----------------------|----------------------------------|-----------------------------------|---------------------------------|-----------------------|------------------------------|
| 1 | 265 | 176 | 30 | 575 | 451 | 50 |
| 1.5 | 430 | 283 | 20 | 511 | 459 | 51 |
| 2 | 560 | 369 | 15 | 475 | 445 | 49 |
| 2.5 | 710 | 468 | 8 | 420 | 403 | 44 |

Height of Burst, y = 210 meters; Scaled Height of Burst, y_1 = 181 meters

V_x meas = 290 m/sec

SECRET

SECRET

(U) The projected velocity along the sea surface plane is calculated to be less than the shock propagation velocity as follows:

$$V_{x \text{ calc}} = U \sin \left(\tan^{-1} \frac{x}{y} \right)$$

As can be seen from Table 5, $V_{x \text{ calc}}$ remains greater than the measured velocity $V_{x \text{ meas}}$.

(S) The above model assumes that the observed effect is in a plane common to the fireball center and the perpendicular to the line of sight. If the disturbance is moving toward the observer at an angle α to the fireball center plane, then the projected velocity would be reduced by a factor of $\cos \alpha$ (see Fig. 24 a). The angle α is not known independently but can be estimated as the angle necessary to reduce $V_{x \text{ calc}}$ to $V_{x \text{ meas}}$. The relationship:

$$\alpha = \cos^{-1} \left(\frac{V_{x \text{ meas}}}{V_{x \text{ calc}}} \right)$$

was used in this determination and the results are tabulated in Table 5 column 7. Plotting the intersection of the angle and the horizontal displacement at a given time, an approximate location for the disturbance is then determined (Fig. 24 b). Although the projected range x was used to calculate the overpressure rather than the actual range $\frac{x}{\cos \alpha}$, the error in these values remains less than $\pm 20\%$. The position found for the disturbance is not exact but does indicate a probable geographic location.

SECRET

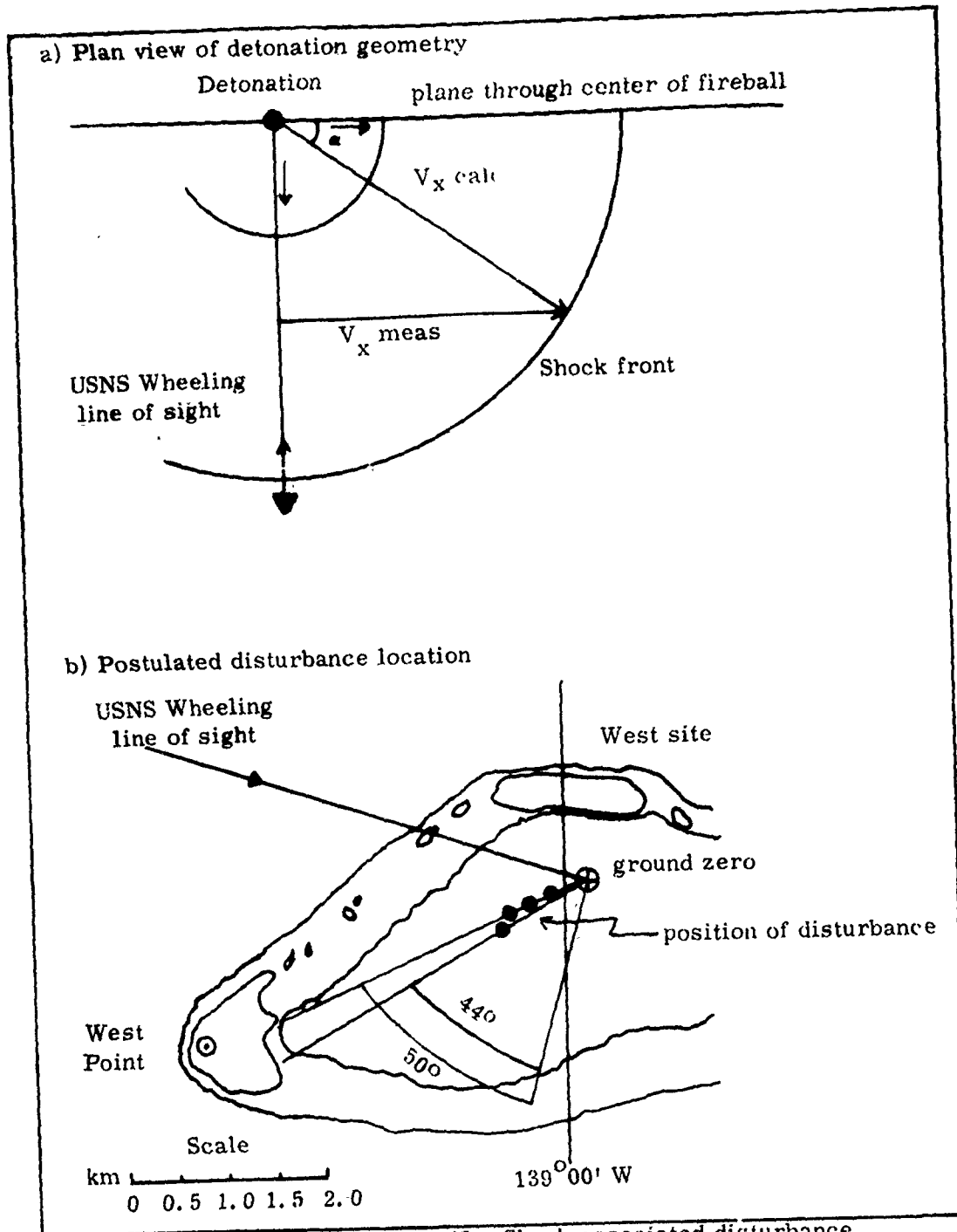


Figure 24 (S). Event Fr 45 - Shock associated disturbance geometry and position (S).

SECRET

SECRET

4.0 RADIOMETRY (U)

4.1 Introduction (U)

(S) The most prominent feature of the debris clouds is the strongly asymmetric nature of their radiative structure, i. e. the existence of luminous patches rather than a relatively uniform fireball. There are two possible explanations for this feature. The observed asymmetries could be a manifestation of asymmetries in the fireball itself, or could be caused by the fireball being covered with an intermittent layer of cooler debris, such as soil or water, which have areas of varying opacity. Each of these possibilities incorporates different implications about what might be learned about the fireball from the data at hand. However, neither explanation can be applied to the present observations without reference to a physically more comprehensive fireball model, such as is incorporated into large computer codes.

(S) In this section the results of measurements made upon the luminous patches are presented. These measurements were made without regard to a particular physical model of the structure of the whole fireball and were made primarily for the benefit of radar experimenters to aid in the interpretation of their experiments.

4.2 Luminous Area vs. Time (U)

(U) The areas of the most prominent luminous features were determined as a function of time by tracing the outlines of such features from photographic prints of records obtained with the Mitchell cine camera operated at 100 frames per second. Enlarged outlines of the selected luminous

SECRET

(U)

features are shown in Figures 25 - 28. These outlines correspond to the photographs shown previously in Figures 3, 6, 7, and 10. The horizon is represented by a long line.

(S) The outlines were scanned with a planimeter in order to measure the total area for each time frame. The area at the source is presented as a function of time in Figures 29 - 31 for the three nuclear events. It should be noted that these values represent projections of object areas upon the film plane and not areas on the curved surface of the cloud itself. Note that the vertical scale changes from Figure 29 to Figure 30. Event Fr. 45, with much greater luminous area than event Fr. 44, reaches a maximum later in time as would be expected from a larger yield. Poor weather obscured event Fr. 46 before it could reach maximum luminous cross section and the final four points are inaccurate since the debris cloud was already partially obscured.

SECRET

SECRET

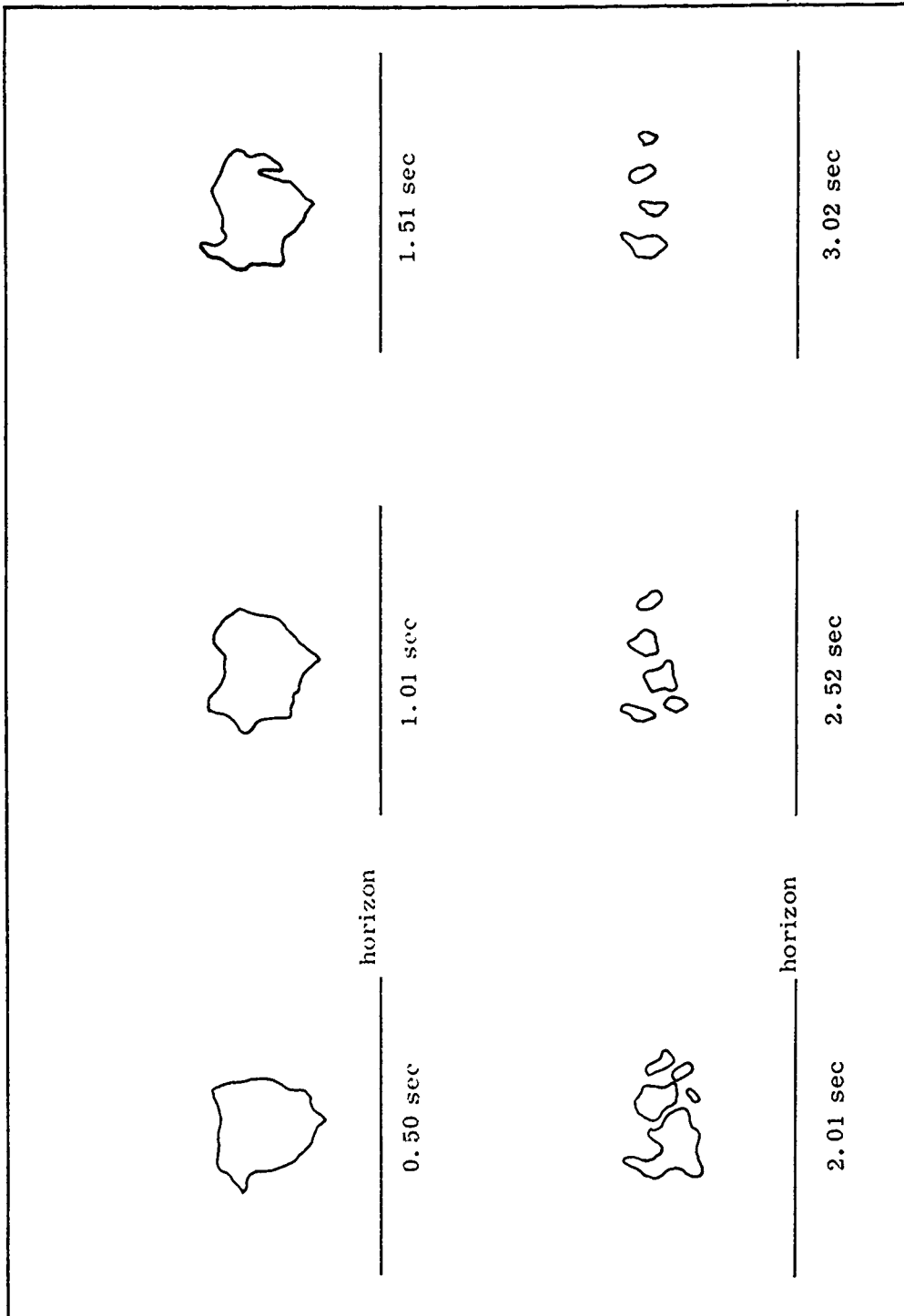


Figure 25 (S). Event Fr 44 - Fireball/debris cloud luminous area outlines; (S) Record 61016; Scale:  = 100 m.

SECRET

SECRET

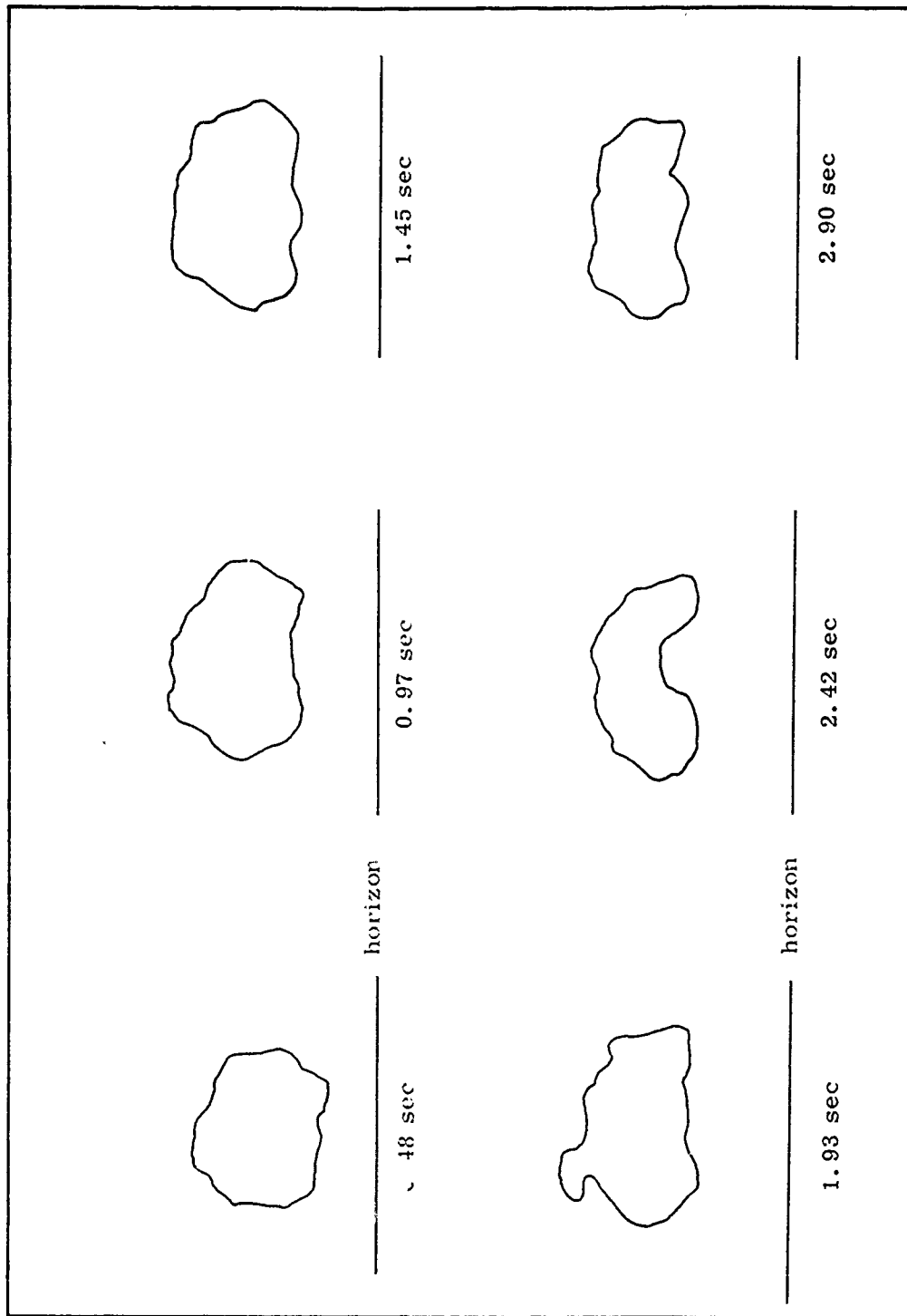


Figure 26 (S). Event Fr 45 - Fireball/debris cloud luminous area outlines; (S) Record 61116; Scale: [] = 100 m.

SECRET

SECRET

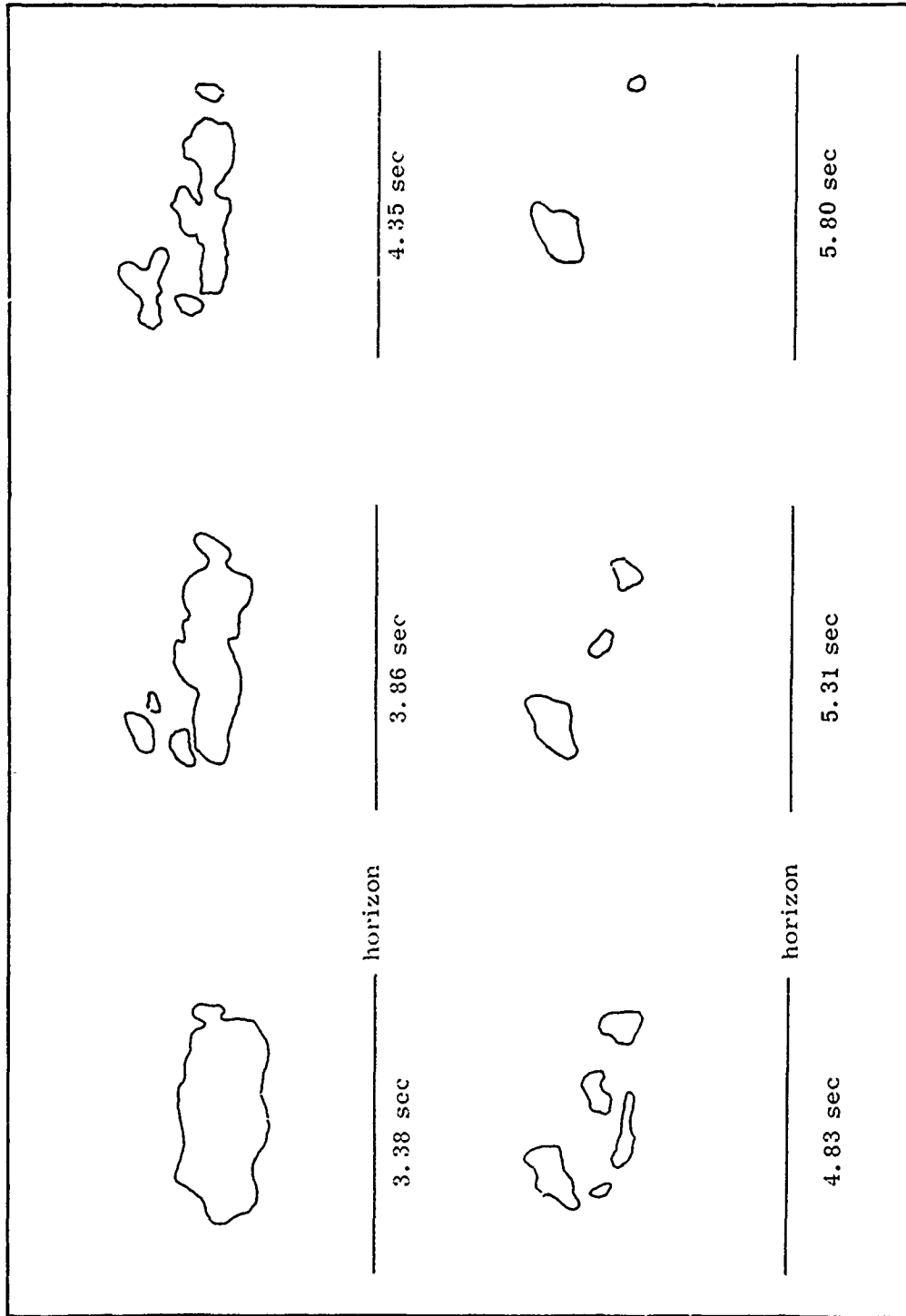


Figure 27 (S). Event Fr 45 - Fireball/debris cloud luminous area outlines; (S) Record 61116; Scale: \square = 100 m.

SECRET

SECRET

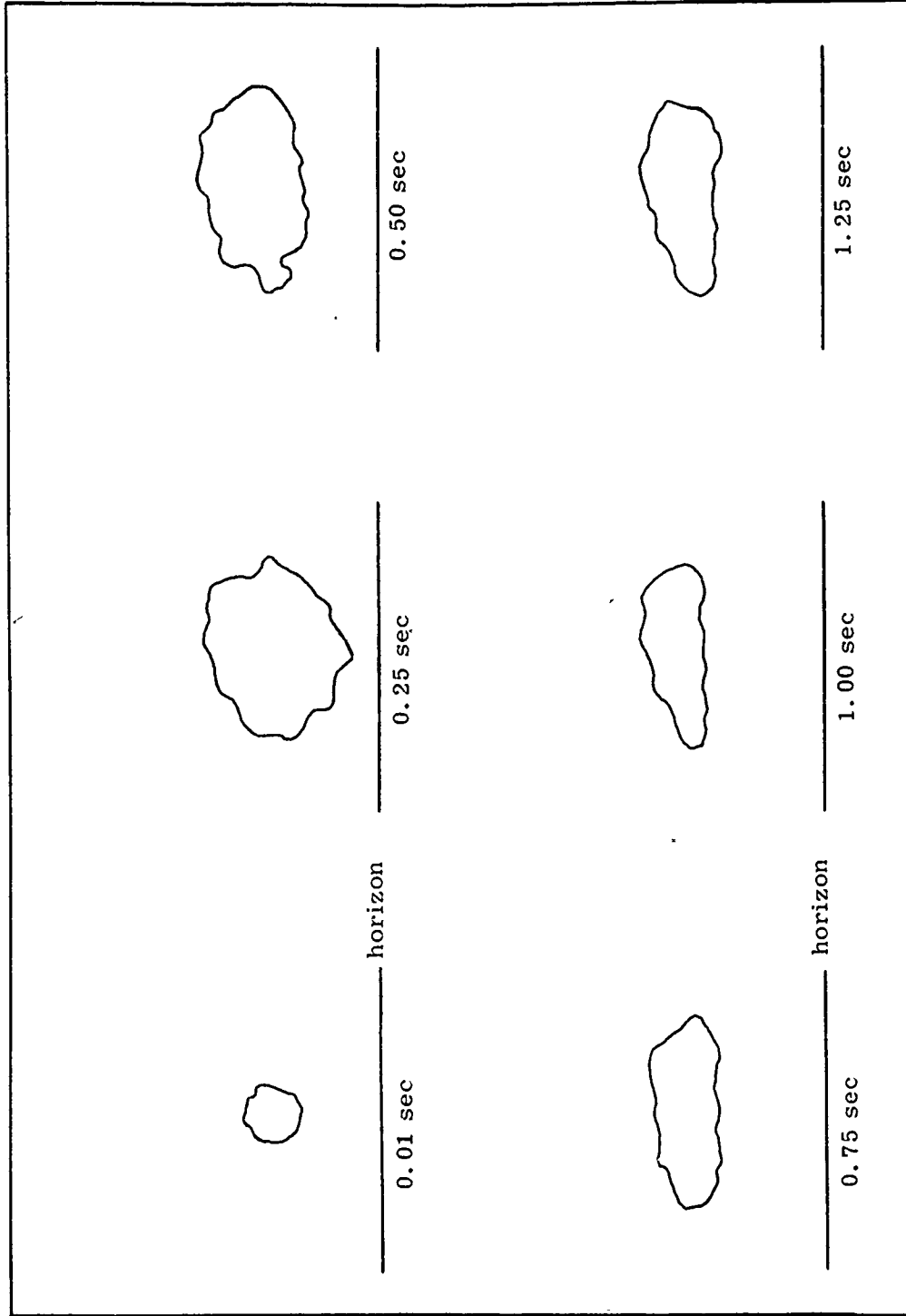


Figure 28 (S). Event Fr 46 - Fireball/debris cloud luminous area outlines; (S) Record 61216; Scale: --- = 100 m.

SECRET

SECRET

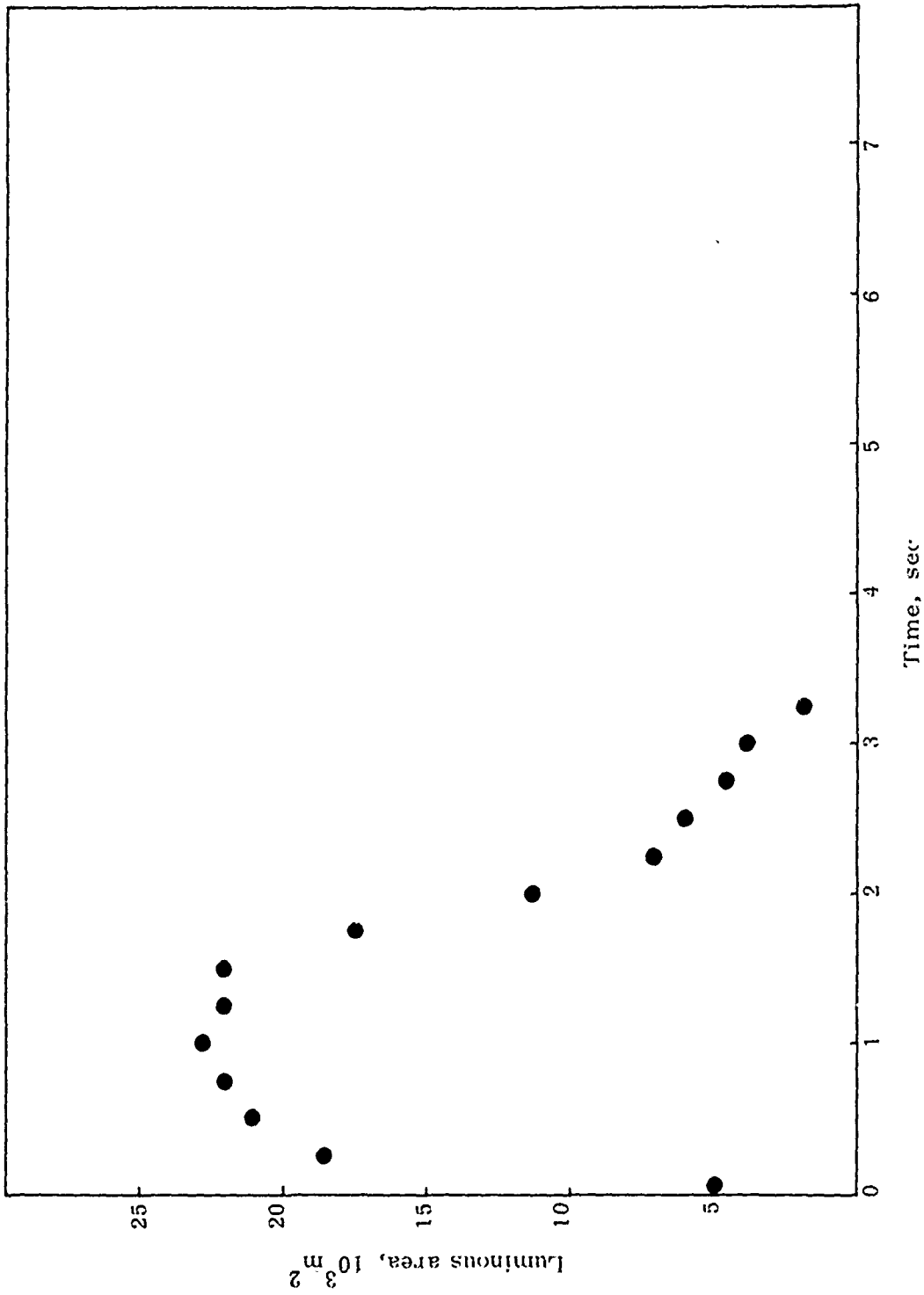


Figure 29 (S). Event Fr 44 - Fireball/debris cloud luminous areas vs. time (S).

SECRET

SECRET

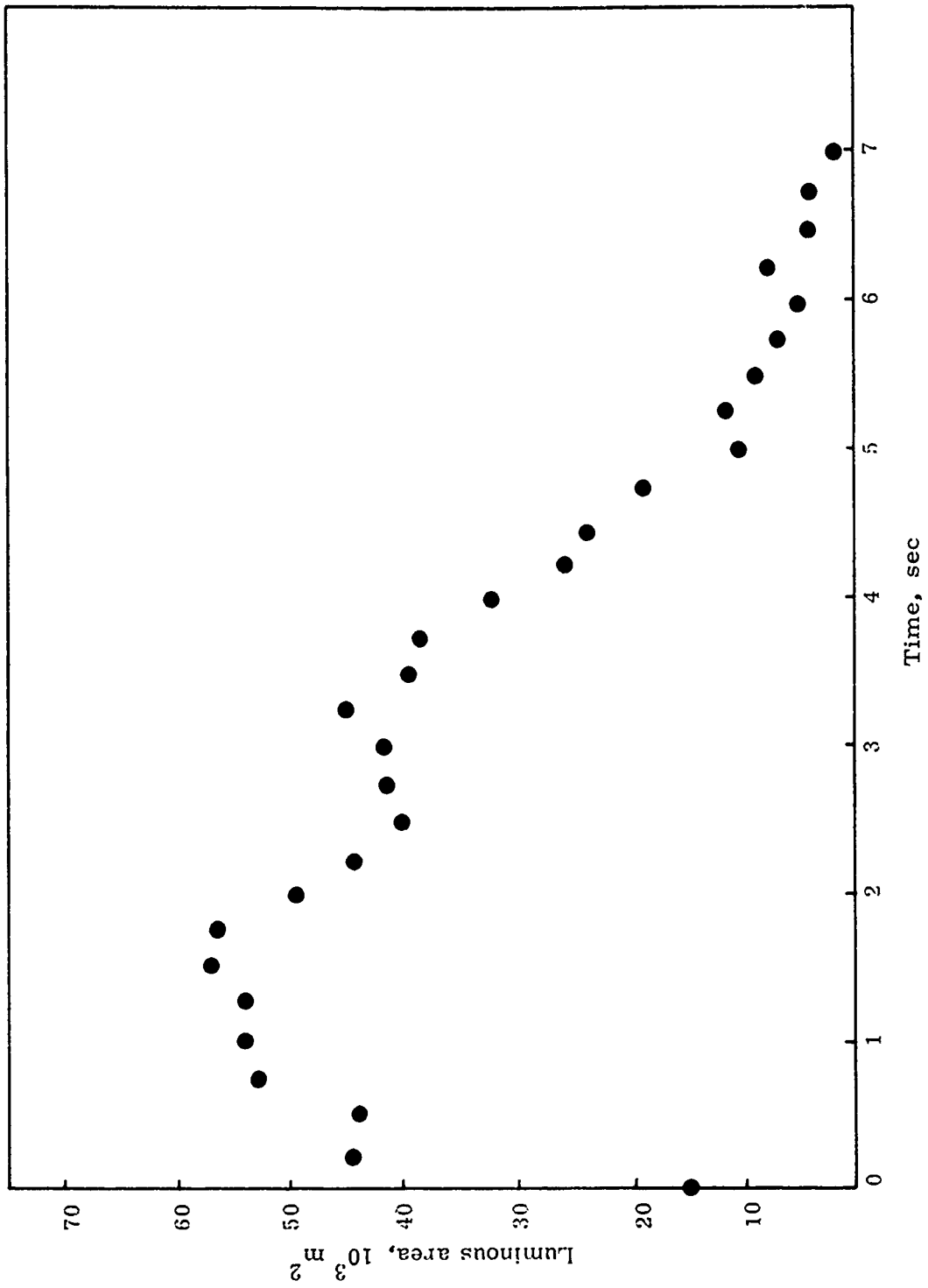


Figure 30 (S). Event Fr 45 - Fireball/debris cloud luminous areas vs. time (S).

SECRET

SECRET

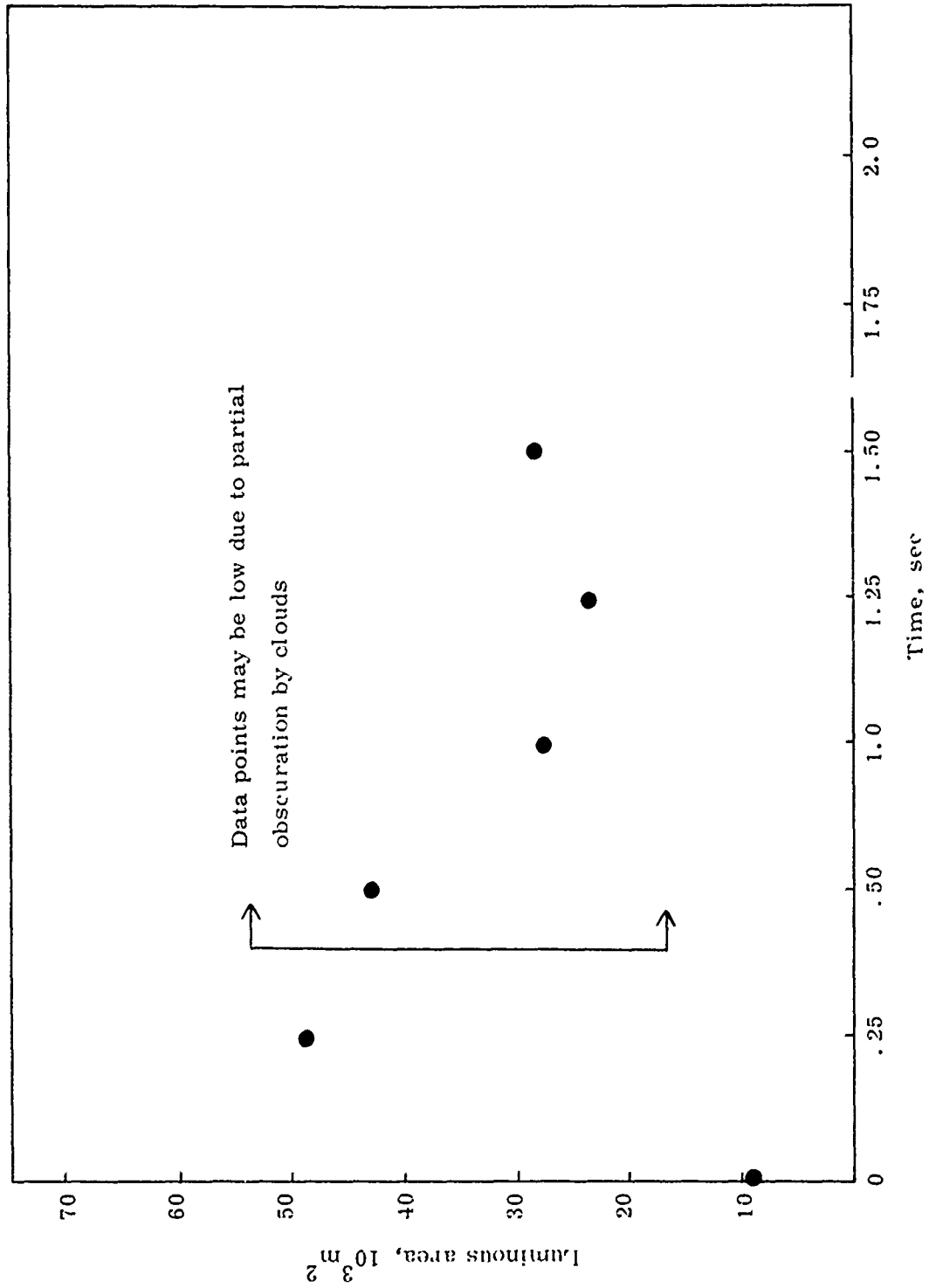


Figure 31 (S). Event Fr 46 - Fireball/debris cloud luminous areas vs. time (S).

SECRET

SECRET

4.3 Constant Density Contours (U)

(U) In addition to the measurements described above, frames of records showing a high degree of image structure were selected for isodensitometric analysis. The process reduces the photographic image to a set of constant density contours. This density map of the original facilitates quantitative analysis of the structure of the image.

(U) The first contour plot, Figure 32, was produced from TIC record no. 61023, a black and white infrared film exposed through a Wratten 88A filter. The selected frame was exposed at H + 3 sec. and contains an image similar to that of Figure 4b. The areas of highest intensity (maximum density) are indicated by a continuous shading technique which makes denser areas darker on the readout.

(S) Two contour plots of TIC record 61123 frame 3, taken at H + 6.2 seconds of event Fr 45 are shown next in Figures 33 and 34. This was also an infrared record exposed through a Wratten 88A filter. The first figure, although smaller, shows the horizon while the second, at a larger scale, shows the image structure more clearly. The protuberance associated with the vaporized support cable is visible on the lower right of the cloud. The dense flat area to the right of the cloud and the light line below the horizon are defects in the film. By counting contour lines, the ratio of densities can be found. For example, with a contour line interval of 0.12 density, from the least to the most dense areas there are approximately 12-13 contour lines which total to an overall density difference of about 1.5. This corresponds to a relative difference in illumination of about 1.5 orders of magnitude.

SECRET

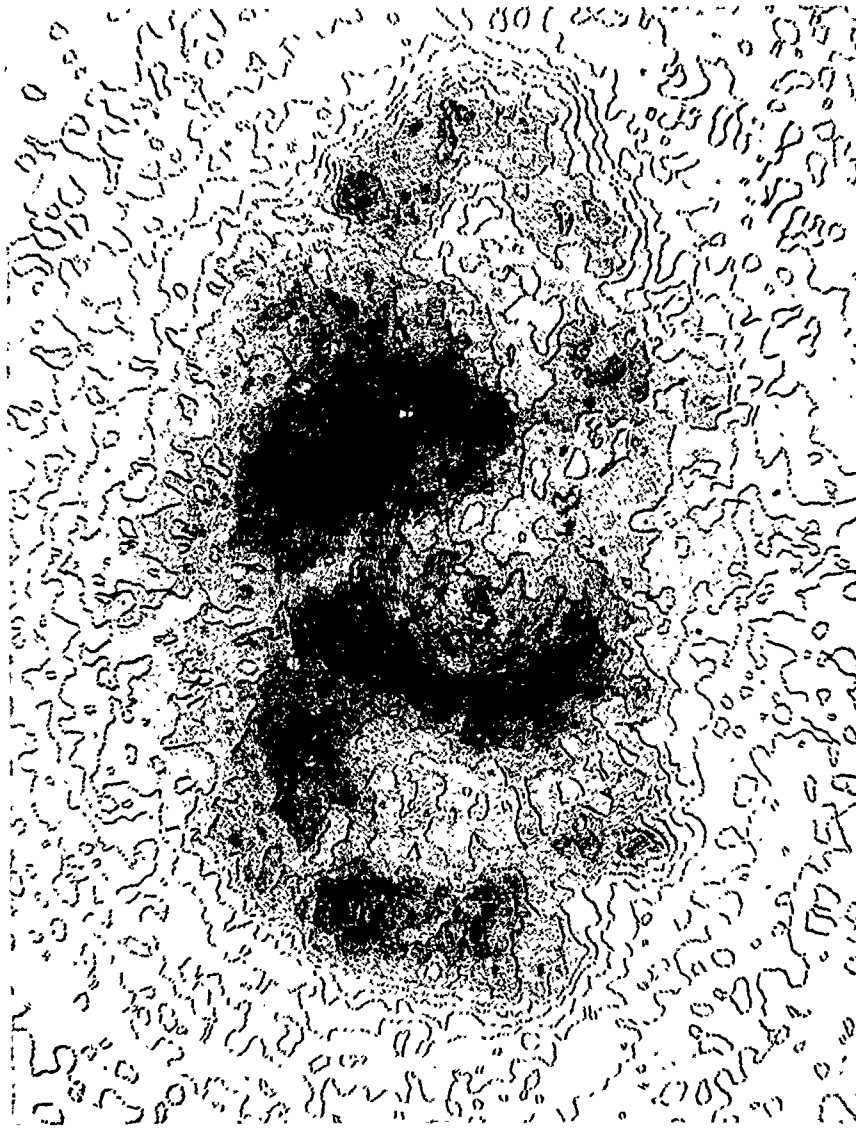
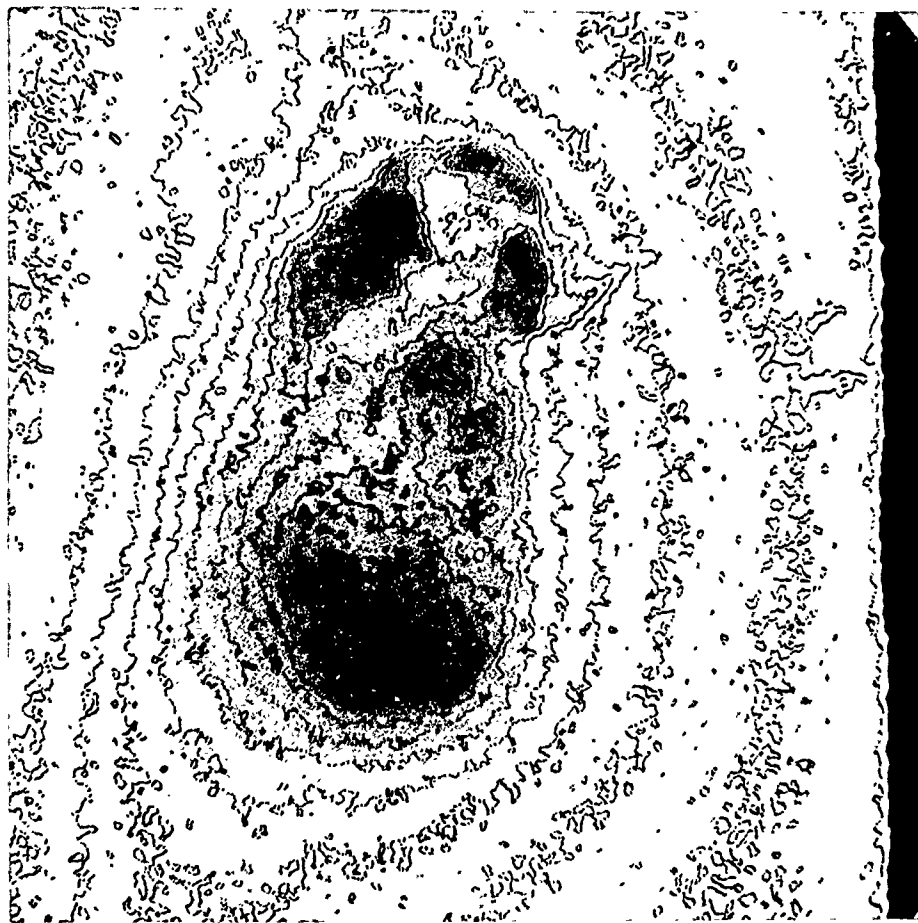


Figure 32 (S). Event Fr 44 - Iso-density contours for frame 61023-2, (S) H+2.8 sec,
Scale:  = 17 m.

SECRET

SECRET



Horizon

Figure 33 (S). Event Fr 45 - Iso-density contours for frame 61123-3, (S) H+6.2 sec,
Scale: [] = 57 m.

SECRET

SECRET

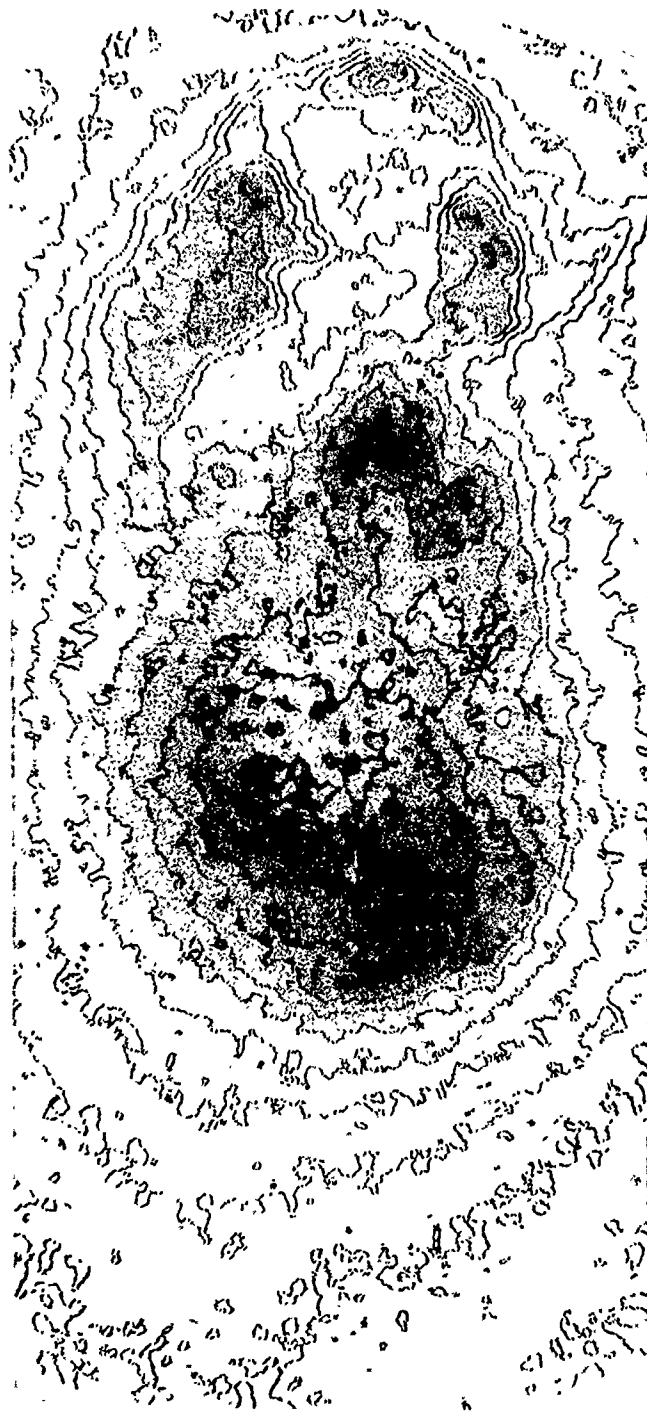


Figure 34 (S). Event Fr 45 - Expanded view of figure 33. (S) Scale: [] = 34 m.

SECRET

SECRET

(S) The records of event Fr. 46 are degraded by rain and obscured by haze. Thus less structural information is available from the isodensity contours of these records. Figure 35 is a contour plot of record 61216 frame 75 exposed at $H + 0.75$ seconds. Figure 36 was produced from record 61223, frame 2 exposed at $H + 2$ seconds and shows the developing Wilson cloud behind the outline of a small French ship.

SECRET



Figure 35 (S). Event Fr 46 - Iso-density contours for frame 61216-75, (S) H+.75 sec,
Scale:  = 89 m.

SECRET

SECRET



Figure 36 (S). Event Fr 46 - Iso-density contours for frame 61223-2, (S) H+2.7 sec,
Scale:  = 165 m.

SECRET

SECRET

4.4 Temperature Determination (U)

4.4.1 Introduction (U)

(S) In this section an attempt is made to estimate the temperature of the debris cloud at a single time during Event Fr 45. This is done by assuming a black body model and utilizing simultaneous color and infrared exposures as a low spectral resolution, wide-band spectrometer. In particular, color and brightness temperatures were calculated for the debris cloud at H + 6.2 seconds.

(U) There are many difficulties in a calculation of this sort and the application of its results, not the least of which are conceptual in nature. It should be emphasized that the application of a black body model to the debris cloud is an enormous simplification of a complex event, a simplification guaranteed to ignore a large amount of useful information. The temperatures thus obtained are approximations. They are intended as an aid in more rigorous investigation of the cloud physics and not as a substitute for it.

(U) Radiation from a given source may be characterized as a combination of two components, thermal emission and non-thermal emission. Non-thermal radiation may consist of discrete lines or a continuum. Thermal emission is radiation due to the source internal kinetic energy, characterized by the temperature of the source. Ideally, thermal emission approaches black body radiation under conditions of thermodynamic equilibrium. Under these equilibrium conditions, spectral radiance (N_λ) due to thermal emission from a source can be described by Planck's black body function as follows:

$$N_\lambda = \frac{c_1}{\pi\lambda^5} \left(e^{c_2/\lambda T} - 1 \right)^{-1} \quad (1)$$

where N_λ is typically measured in units such as ergs/cm²-sec-ster-A.

SECRET

(U) Formula (1) can be inverted to define a brightness temperature, T_B , for given or measured values of N_λ and λ .

$$T_B = \frac{c_2}{\lambda} \left[\ln \left(\frac{c_1 \Delta \lambda}{\pi N_\lambda \lambda^5} \right) \right]^{-1} \quad (2)$$

(U) Planck's formula can also be used to compare or predict the ratio of radiances at different wavelengths:

$$\frac{N_{\lambda 1}}{N_{\lambda 2}} = \left(\frac{\lambda_2}{\lambda_1} \right)^5 \left(\frac{e^{c_2/\lambda_2 T} - 1}{e^{c_2/\lambda_1 T} - 1} \right) \quad (3)$$

(U) This equation defines a color temperature, T_c , the temperature at which a black body would produce the same distribution of energy between the two wavelengths in question. An example of this principle is the use of B-V magnitudes to classify stars on H-R diagrams in astronomy. Note that color temperatures have the advantage of requiring only relative rather than absolute measurements of radiance, thus minimizing the effect of other uncertainties in the measurement process.

(U) The third type of temperature associated with black bodies, the effective temperature, T_e , is defined by the total spectrally-integrated radiance of the black body:

$$\int_0^\infty N_\lambda d\lambda = \sigma/\pi T_e^4 \quad (4)$$

where σ is the Stefan-Boltzmann constant. This temperature is not considered here because of spectral limitations of the instrumentation used and the uncertainties in the transmission properties of the atmosphere.

SECRET

(S) The usefulness and relevance of these definitions to actual fireballs depends partly on how well the fireball can be modeled as a black body. Although the debris cloud cannot be considered to be in thermodynamic equilibrium, it is common to regard such structures as composed of small volumes, each one of which is in local thermodynamic equilibrium. Making this assumption, the radiation received from the surface of the cloud may be a useful indicator of the thermal conditions there. In addition, other high-resolution spectrographic observations have shown that the fireball radiation is dominated by continuum rather than line emission, thus lending some validity to the temperature concepts employed here.

4.4.2 Radiance Measurements (U)

(S) Suitable complementary records were first identified. The films chosen for analysis were a 5-inch Ektachrome MS record (TIC #61122), and a 5-inch Infrared Aerographic record (TIC #61123) made through a Wratten 88A filter. These films give a combined spectral coverage from 4000 to 9000 Å. The films were recorded through identical 215mm focal length lenses. The two frames were exposed within 20ms of each other for 14ms at H + 6.2 seconds during event Fr 45. This is the first time at which the fireball images are not overexposed or degraded by Wilson cloud scattering. At this time, the cloud has much visible structure, including a pronounced darkening in the center and across the bottom half of the cloud (see Figures 33 and 34).

(U) Wavelengths for 4-color radiometry were selected to coincide with the peaks of the Kodak sensitivity curves for the blue, green, and red layers of EMS film, and the peak of the response function created by convolving the sensitivity curve of the IR film with the transmission curve of the W88A filter. The measured radiance in each layer was divided by the band width

SECRET

UNCLASSIFIED

(U)
of the layer's response to obtain band-averaged spectral radiances needed for temperature calculations. Bandwidths for the four color layers were determined by using the width of the layer sensitivity curves at 1/10 peak sensitivity. In the case of the IR film, the half-power point of the combined film-filter curve was used because of the broader nature of that particular curve. Table 6 lists the different layers, their band limits, and peak wavelengths.

(U) The films were calibrated by means of density scales which were placed on the film and processed with data records. A density scale is a series of calibrated exposures made on the film by exposing it to a known light source through an array of neutral density filters. The resultant density steps are scanned with a microdensitometer to obtain a correlation between density and relative exposure. The Infrared Aerographic record was processed along with a density scale made on the IF film by a 2850° K lamp exposed through a Wratten 88A filter to simulate the data acquisition conditions. The color film was processed without a scale initially but with accurately known processing conditions. Density scales were later applied to film stock of the same emulsion which was then processed under the same conditions used to process the original record.

(U) To calibrate the scales, the spectral output of the sensitometer (lamp plus transmissions of all filters in the optical train) was integrated over each of the four bandwidths mentioned above. For the purpose of these calculations, the sensitivity curves were assumed to be square waves with the wavelength limits indicated in Table 6.

UNCLASSIFIED

TABLE 6. (U) SPECTRAL RESPONSE LIMITS OF
EKTACHROME MS AND INFRARED AEROGRAPHIC FILMS (U)

| Layer | Band Limits (A) | Peak Wavelength (A) | Wavelength Interval $\Delta\lambda$ (A) |
|---------|-----------------------|---------------------------|--|
| Blue | 4000 - 5000 | 4200 | 1000 |
| Green | 5100 - 5900 | 5500 | 800 |
| Red | 6000 - 7000 | 6500 | 1000 |
| IR/W88A | 7400 - 8800 | 8100 | 1400 |

UNCLASSIFIED

(U) Density measurements of the step scales and data frames were made on a Jarrell-Ash microdensitometer which has a one-dimensional automatic scanning capability. The scanning process was performed three times for each scan-line on color film, once for each layer, with a Wratten 92, 93, or 94 filter and Kodak 301 glass infrared cut-off filter installed in the optical train of the machine to isolate the three color layers. Procedures associated with calibrating the machine made it necessary to move the film each time a different filter combination was installed, thus, although features on the image, such as the horizon, were used for reference, registration uncertainties were introduced into the process. Absolute H & D curves for each bandwidth were derived from the step scale scans and are shown in Figure 37. No attempt was made to separate integral and analytical densities.

(U) The data frames were scanned parallel to the horizon at distances of 2.0, 2.7, and 3.3 mm above the horizon. The initial visual inspection of the IR record had placed the center of the cloud at 2.7 mm above the horizon. However the middle scan, which is reduced and discussed in this report, appears slightly above the center of the cloud in Figure 38 taken from the IR record.

(U) The measured densities were converted to exposures using the H & D curves. Exposures were converted to radiance by the expression:

$$N = \frac{4}{\pi} (f/n)^2 \frac{1}{\tau_a} \frac{1}{\tau_l} \frac{1}{\tau_f} \frac{1}{\tau_t} E \quad (5)$$

which is accurate for images near the center of the optical axis. In this expression, exposure, E, is expressed in ergs/cm², radiance, N, is the integrated spectral radiance for each bandwidth, expressed in ergs/cm²-sec-ster, t is the exposure time, (f/n) is the f-number of the lens, and $\tau_{a,l,f}$, are the transmittances of the atmosphere, lenses and filters used to record the data.

UNCLASSIFIED

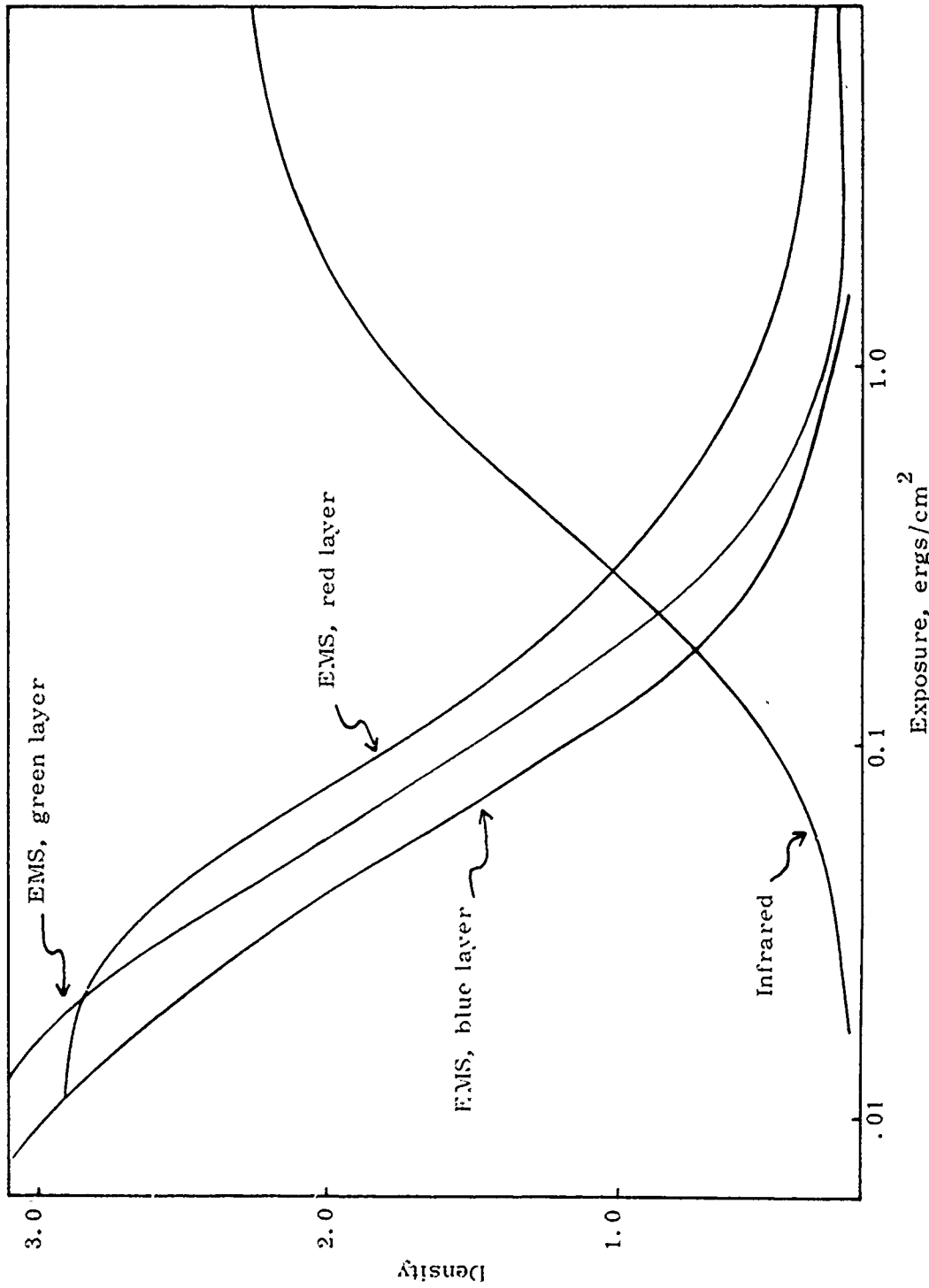


Figure 37 (1). Characteristic curves for Ektachrome MS and Infrared Aerographic films (U).

UNCLASSIFIED

SECRET



Figure 38 (S) Event Fr 45 - Frame 61123-3 with Radiance Scan Line (S)

Scale:  = 100 m.

SECRET

SECRET

(U) The lens transmission was assumed to be 0.8 for all cases. The W88A filter transmission was obtained from Kodak published data. Atmospheric transmissions were calculated for each nominal wavelength from AFCRL published data and Allen (References 4, 5, 6). The results of these calculations (as described in Appendix D) for a 20 mile horizontal path length over water were:

| λ | τ_a |
|-----------|----------|
| 8100 | .69 |
| 6500 | .57 |
| 5500 | .47 |
| 4200 | .15 |

(S) After computing the radiance, in order to calculate the cloud's temperature, it is necessary to correct for sunlight reflected from the cloud's surface, since reflected sunlight will more nearly approximate the sun's color temperature than the cloud's. It was decided to use the radiance of background meteorological clouds as a measure of the amount of reflected radiation from the fireball cloud. This method has several drawbacks: first, the greater distance of the background clouds which introduces an error due to increased atmospheric attenuation; second, the necessary assumption that the two clouds are of sufficiently similar material and reflectance; third, fluctuation in the background which makes it difficult to assign a background level.

(S) The last consideration is crucial with regard to fireball radiances derived from the blue layer. In this layer the radiance due to natural light constitutes 90% of the total signal. Thus a 5% deviation in background level produces a 50% error in the calculated source radiance. Because of this potential error, radiances from the blue layer were not used in the temperature calculations.

SECRET

(U) Radiance profiles through the center of the cloud were produced, taking all of the above into consideration, for each color on different pieces of paper and then overlaid by eye. The resulting profiles are shown in Figure 39. The radiances shown are the integrated radiances over each bandwidth, which is identified by its central wavelength. In registering the radiance profiles, the best overall fit was attempted rather than lining up any one feature precisely. The gross features of the curves seem consistent, the differences in fine structure may be due to a 0.1 mm uncertainty in the horizontal position of the scan line from color to color.

4.4.3 Temperature Calculations (U)

(U) Color and brightness temperatures, from green, red, and IR radiance values, were calculated using the black body approximation discussed in section 4.4.1. The spectral radiance for a black body is given by:

$$N = \frac{c_1}{\pi \lambda^5} \left(e^{c_2/\lambda T} - 1 \right)^{-1} \quad (6)$$

where

T = Absolute temperature of the radiating body ($^{\circ}\text{K}$)

λ = Wavelength in centimeters

$c_1 = 2 c^2 h = 3.74 \times 10^{-12}$ watt cm^2

$c_2 = hc/k = 1.439$ cm $^{\circ}\text{K}$

For the situation $e^{c_2/\lambda T} \gg 1$, equation (6) can be approximated as

$$N = \frac{c_1}{\pi \lambda^5} e^{-c_2/\lambda T} \text{ watts/cm}^2/\text{cm} \quad (7)$$

which is known as Wien's Displacement Law.

SECRET

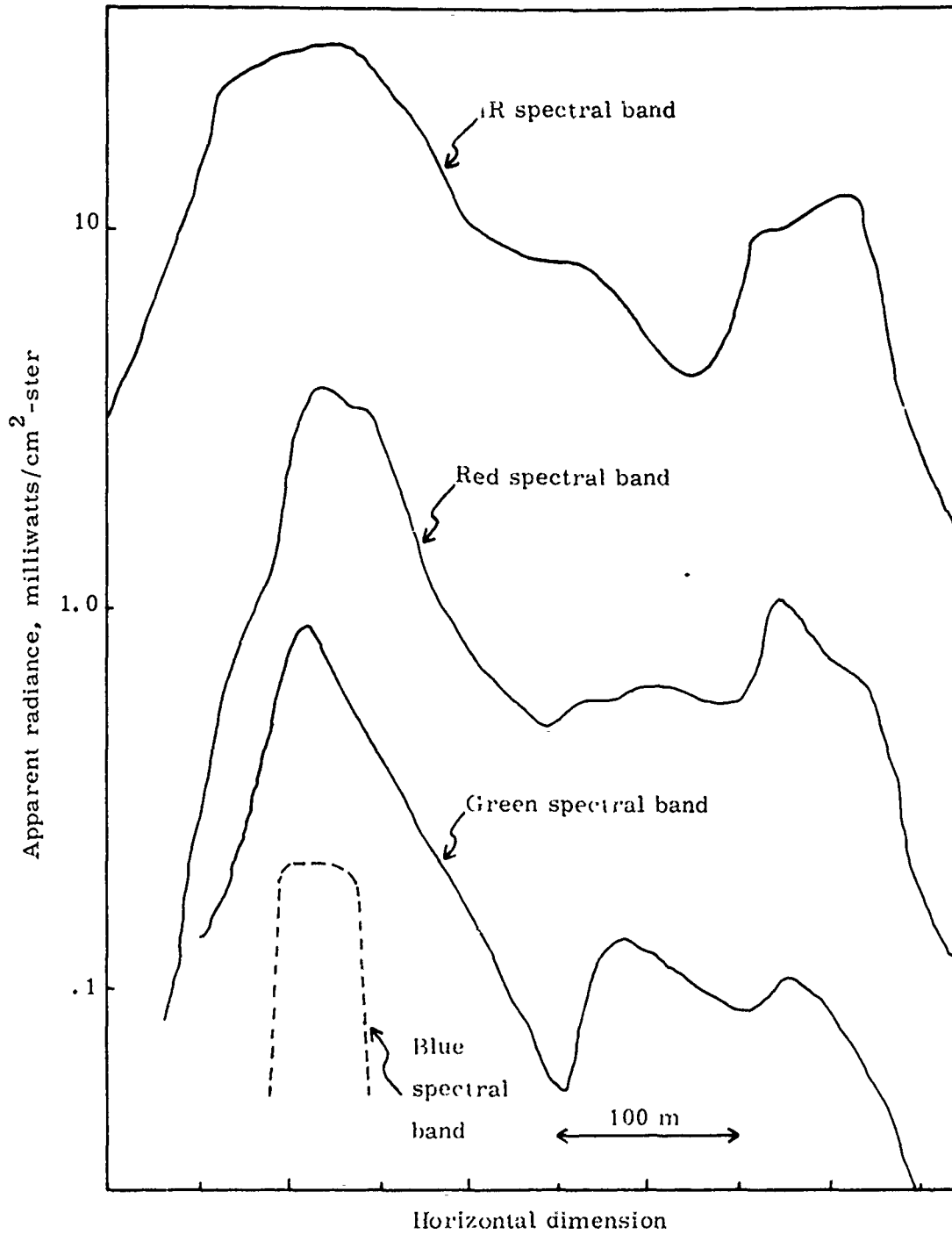


Figure 39 (S). Event Fr 45 - Measured luminous cloud radiance profiles (S).

SECRET

SECRET

(U) In order to check this approximation, a sample calculation with a temperature of 1500°K and a wavelength of 6000 A yields:

$$\frac{c_2}{\lambda T} = \frac{1.44 \text{ cm } ^\circ\text{K}}{6 \times 10^{-5} \text{ cm} \times 1.5 \times 10^3 \text{ } ^\circ\text{K}} = 16$$

and $e^{16} \gg 1$. Therefore equation (7) is a good approximation for the conditions expected in these calculations. The expressions for the brightness and color temperatures then become:

$$T_B = \frac{c_2}{\lambda} \left[\ln \left(\frac{c_1 \Delta \lambda}{\pi N \lambda^5} \right) \right]^{-1} \quad (8)$$

$$T_c = \frac{c_2 \left(\frac{1}{\lambda_2} - \frac{1}{\lambda_1} \right)}{\ln \left[\frac{N_1}{N_2} \frac{\Delta \lambda_1}{\Delta \lambda_2} \left(\frac{\lambda_1}{\lambda_2} \right)^5 \right]} \quad (9)$$

(S) Figure 40 shows a temperature profile of the cloud based on the average of the IR/red, red/green, and IR/green color temperatures. It can be seen that the temperatures ranged from just under 1800°K to about 800°K, and within the cloud structure, relative differences of around 400°K are evident. This profile bears a fair resemblance to the general shape of the radiance profiles with a few important exceptions. Where the IR curve shows a deep trough, the temperature curve shows a hump, and where the IR curve shows a hump - on the extreme right - the temperature curve shows a rapid decrease.

(U) Physically, one would expect an increase in intensity to correspond to an increase in temperature. However, with color temperatures, it is the ratio of the intensities at different wavelengths which are important. The left-hand peak appears to grow wider and broader as one goes to longer wavelengths. Going from left to right across the radiance profiles,

SECRET

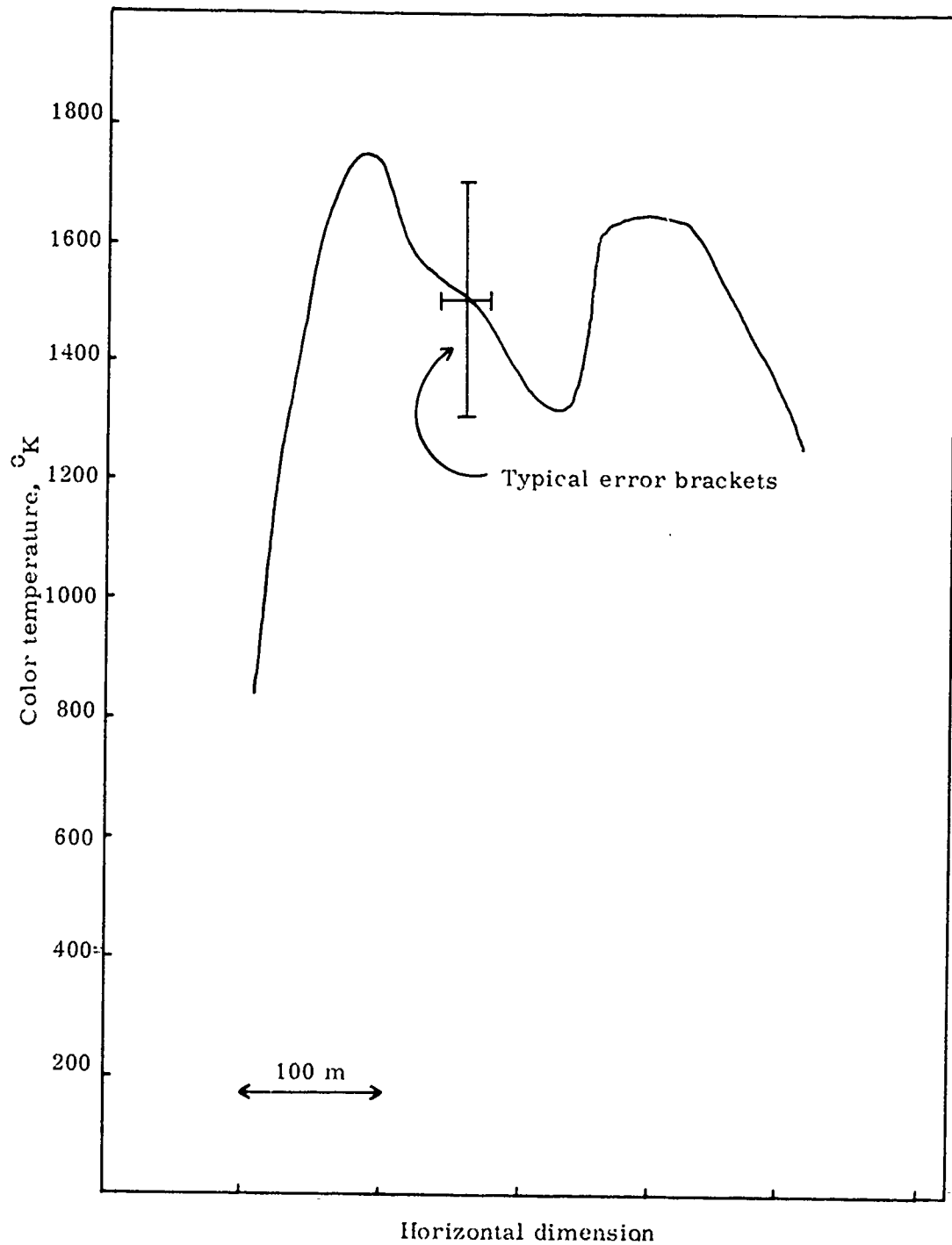


Figure 40 (S). Event Fr 45 - Calculated cloud color temperature profile (S).

SECRET

SECRET

(U)

it can be seen that the IR undergoes a larger increase from trough to peak than does the red or green, thus reddening the light and making it appear cooler even though it is brighter. The color temperatures are quite sensitive to the relative placement of the profiles so that a small horizontal shift of one curve can cause radical changes, particularly on the edges of the cloud image. The uncertainty in horizontal placement is estimated to be about $\pm .1$ mm on the film (corresponding to about 15m at the source), represented by the horizontal error bracket in Figure 40.

(U) Within these limits it is difficult to establish the temperature structure of the cloud in detail with great confidence. However, the gross temperature structure of the cloud seems more evident. The cloud appears to have two hot spots with a cool region in between. A simplified model of the cloud appears in an unscaled form in Figure 41. Using this model of the cloud, a corresponding temperature distribution was computed using only the radiance values of the two major peaks and the trough of each color profile. Brightness temperatures for the three features, and color temperatures for the three ratios were combined to give an average brightness temperature and an average color temperature for each section of the cloud as presented in Table 7. In general, the color temperatures are 100-150^o hotter than the brightness temperatures for this model.

(S) It should be mentioned that the inclusion of the blue layer into these computations would have the overall effect of raising temperatures by 200-300 degrees. The blue-green color temperatures in particular are consistently higher than the others. The blue-green color temperature corresponding to the left-hand peak is 2800 degrees although the blue brightness temperature of the left-hand peak is only 1882. The blue radiance values were considered more suspect than the others for reasons mentioned earlier and therefore were omitted from the calculations. With blue included, color temperatures for T_1 , T_2 , and T_3 would be:

SECRET

SECRET

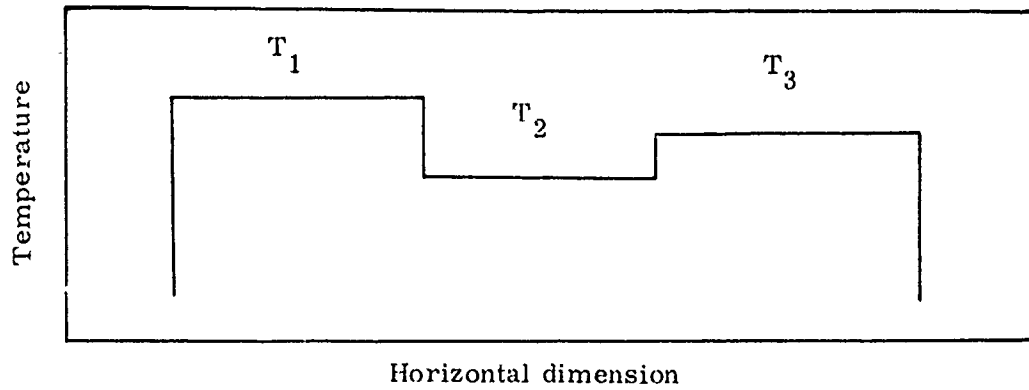


Figure 41 (S). Event Fr 45 - Simplified temperature model of cloud (S).

TABLE 7 (S). TEMPERATURE ASSOCIATED WITH SIMPLIFIED MODEL (U).

Brightness temperatures

| | λ | T_1 | T_2 | T_3 |
|-------------|-----------|-------|-------|-------|
| \bar{T}_B | 8100 | 1581 | 1359 | 1436 |
| | 6500 | 1560 | 1372 | 1434 |
| | 5500 | 1614 | 1374 | 1443 |
| | | 1585 | 1368 | 1438 |

Color temperatures

| | λ_1/λ_2 | T_1 | T_2 | T_3 |
|-------------|-----------------------|-------|-------|-------|
| \bar{T}_C | 8100/6500 | 1587 | 1237 | 1591 |
| | 6500/5500 | 1920 | 1406 | 1662 |
| | 5500/8100 | 1724 | 1302 | 1624 |
| | | 1744 | 1315 | 1626 |

SECRET

(S)

$$\begin{aligned}T_1 &= 2092^\circ\text{K} \\T_2 &= 1315^\circ\text{K} \\T_3 &= 1966^\circ\text{K}\end{aligned}$$

4.4.4 Discussion (U)

(U) It is important to realize that the brightness temperature is a relatively insensitive function of the radiance. Just how insensitive this dependence is in the regions in which the preceding calculations have been performed can be seen by performing a sample calculation. Consider two sources, one at 1200°K and the second at 1800°K , and calculate the ratio of their spectral radiances at 6000\AA . Using the Wien displacement law,

$$\frac{N(T_2)}{N(T_1)} = \frac{e^{-c_2/\lambda T_2}}{e^{-c_2/\lambda T_1}} = e^{c_2/\lambda \left(\frac{T_2 - T_1}{T_1 \times T_2} \right)}$$

Using $T_2 = 1800^\circ\text{K}$ and $T_1 = 1200^\circ\text{K}$

$$\frac{N(T_2)}{N(T_1)} = e^{6.7} \approx 800$$

(U) Thus, in these conditions, a temperature spread of 600°K changes the radiance by about three orders of magnitude. The dynamic range of color and infrared film combined appears to be about 500, with a temperature change of 600°K straining the limits of the film. Conversely, the presence of an exposed image in a given layer of the film would seem sufficient to define the temperature of the source to within about two hundred degrees. It should be noted, however, that as the temperature increases the range in temperature which the film can record also increases. Likewise, at longer wavelengths, the ratio $N(T_2)/N(T_1)$ also decreases.

SECRET

(U) The largest uncertainty in the radiance measurements results from the uncertainty in atmospheric transmission due to lack of hard data concerning the number of aerosols present (see Appendix D). The effect of this uncertainty can be gauged by re-constructing the transmission for an aerosol content ten times the concentration assumed above, (about half, therefore, of the 23 km visibility case), thus obtaining the following changes in transmission:

| λ | τ_a | τ_a for 10 Na |
|-----------|----------|--------------------|
| 4200 | .15 | .008 |
| 5500 | .47 | .038 |
| 6500 | .57 | .050 |
| 8100 | .69 | .081 |

As can be seen, an order of magnitude change in τ_a results. This in turn leads to an order of magnitude change in radiance. This, however, will only lead to a change in the brightness temperature of around 50° , or less than 5 percent. The ratios between the transmission coefficients for different colors show a much smaller deviation than the transmission themselves, thus altering the color temperatures to an even smaller degree. Therefore, uncertainty in atmospheric transmission data does not introduce an appreciable error into the temperature calculations.

UNCLASSIFIED

LIST OF REFERENCES (U)

1. Donald Kerr, "Operation Garza", Oct. 1972, Los Alamos Scientific Laboratory Report LA-5066-PR, pg. 6, Secret - Restricted Data.
2. Nathaniel Bowditch, LL. D., "American Practical Navigator", 1966, U. S. Government Printing Office, Washington, D. C., pg. 1187, Unclassified.
3. Defense Nuclear Agency, Capabilities of Nuclear Weapons, 1972, Washington, D. C., ch 2, Secret - Restricted Data.
4. Shea L. Valley, Ed., "Handbook of Geophysics and Space Environments", 1965, McGraw Hill, New York, Unclassified.
5. McClatchey et al, "Optical Properties of the Atmosphere", 24 August 1972, Air Force Cambridge Research Laboratories, AFCRL-72-0497, Unclassified.
6. C. W. Allen, "Astrophysical Quantities", Second Edition, 1963, University of London Press, London, pg. 122, Unclassified.
7. Rhodes Fairbridge, Ed., "The Encyclopedia of Atmospheric Sciences and Astrogeology", 1967, Reinhold Publishing, New York, pg. 88, Unclassified.

CONFIDENTIAL

APPENDIX A

INSTRUMENT PLAN (U)

(U) The camera systems employed for data collection during Operation Dial Flower are presented in Appendix A. Parameters relevant to each camera such as focal length, framing rate, field of view and nominal running time are included. Only those filters are included which alter the spectral range of the light incident on the film are listed whereas neutral density filters are not listed as they change from one event to another. A list of the film types and their abbreviations found in both the instrument plan and the data record summary follows:

| CODE | DESCRIPTION | TYPE NO. | NOMINAL ACA |
|-------|-------------------------|----------|----------------|
| ACN | Aerocolor Negative | 2445 | 230-320 |
| AIR | Aerochrome Infrared | 2443 | 100 |
| CPS | Ektacolor Professional | 5056 | 100 |
| EMS | Ektachrome Medium Speed | 5256 | 64 |
| HIR | High Speed Infrared | 2481 | 80 |
| IRA | Infrared Aerographic | 2424 | 80 |
| KR II | Kodachrome II | 7265 | 25 |
| PXN | Plus-X Negative | 7231 | 80 |
| XRM | Extended Range Modified | SO-167 | Wide Latitude |

CONFIDENTIAL

TABLE A-1 (C)
 TECHNOLOGY INTERNATIONAL CORPORATION
 INSTRUMENT PLAN (U)

OPERATION: DIAL FLOWER DATE: Summer 1972 STATION: USNS WHEELING
 EVENT: ALL LOCATION: OFF-CONTINENT PROJ/ENGINEER: DEUEL

| POSITION | INSTRUMENT | FOCAL LENGTH | FILTER | FILM | NOM. RUNNING | | |
|----------|-------------|--------------|--------|-------------------------|--------------|--------------|---------------|
| | | | | | TIME | SHUTTER/RATE | FIELD OF VIEW |
| 11 | AN-N6 | 35mm | - | KR II 16mm x 50' | 125 sec | 16 fps | 12° x 17° |
| 12 | AN-N6 | 76mm | - | KR II 16mm x 50' | 62 sec | 32 fps | 6° x 8° |
| 13 | AN-N6 | 35mm | - | XRM/KR II 16mm x 50' | 31 sec | 64 fps | 12° x 17° |
| 14 | AN-N6 | 35mm | W88A | HIR 16mm x 50' | 125 sec | 16 fps | 12° x 17° |
| 15 | PS-16-1B | 50mm | - | XRM 16mm x 200' | 13/10sec | 600/800 fps | 8.6° x 12° |
| 16 | HS Mitchell | 80mm | - | PXN 35mm x 100' | 64 sec | 100 fps | 12.8° x 17° |
| 17 | AN-N6 | 100mm | - | KR II/XRM 16mm x 50' | 31 sec | 64 fps | 4° x 6° |

ADDITIONAL INFORMATION:

CONFIDENTIAL

CONFIDENTIAL

TABLE A-1 (cont.) (C)
TECHNOLOGY INTERNATIONAL CORPORATION
INSTRUMENT PLAN (U)

OPERATION: DIAL FLOWER DATE: Summer 1972 STATION: USNS WHEELING
 EVENT: ALL LOCATION: OFF-CONTINENT PROJ./ENGINEER: DEUEL

| POSITION | INSTRUMENT | FOCAL LENGTH | FILTER | FILM | NOM. RUNNING TIME | SHUTTER/RATE | FIELD OF VIEW |
|----------|------------|--------------|----------|----------------------|-------------------|--------------|---------------|
| 21 | B-C/E | 105mm | - | EMS 70mm x 100' | 60 min | 2 - 15 sec | 40° x 30.5° |
| 22 | K-46B | 215mm | - | EMS/CPS 5" x 150' | 60 min | 2 - 15 sec | 30° x 30° |
| 23 | K-46B | 215mm | W88A | IRA 5" x 150' | 60 min | 2 - 15 sec | 30° x 30° |
| 24 | K-17D | 500mm | - | EMS 9 1/2" x 125' | 150 frames | Manual | 25° x 25° |
| 25 | K-17D | 914mm | - | EMS 9 1/2" x 125' | 150 frames | Manual | 14° x 14° |
| 31 | B-C/E | 105mm | W12/W88A | AIR 70mm x 100' | 60 min | 2 - 30 sec | 40° x 30.5° |
| 32 | K-17D | 154mm | - | EMS 9 1/2" x 300' | 60 min | 2 - 30 sec | 73.7° x 73.7° |
| 33 | K-17D | 154mm | W88A | IRA 9 1/2" x 300' | 60 min | 2 - 30 sec | 73.7° x 73.7° |

ADDITIONAL INFORMATION:

CONFIDENTIAL

CONFIDENTIAL

TABLE A-1 (cont.) (C)
 TECHNOLOGY INTERNATIONAL CORPORATION
 INSTRUMENT PLAN (U)

OPERATION: DIAL FLOWER DATE: Summer 1972 STATION: USNS WHEELING
 EVENT: ALL LOCATION: OFF-CONTINENT PROJ/ENGINEER: DEUEL

| POSITION | INSTRUMENT | FOCAL LENGTH | FILTER | FILM | NOM. RUNNING | | | FIELD OF VIEW |
|----------|-----------------------------|---------------|--------|---------------|--------------|--------------|----------------|---------------|
| | | | | | TIME | SHUTTER/RATE | | |
| 41 | Vidicon Camera | 25mm | - | B/W*-VTR 1" | 60 min | 30 fps | 21° x 28° | |
| 42 | Vidicon Camera | 100mm | W88A | B/W*-VTR 1/2" | 60 min | 30 fps | .11° x 14° | |
| 43 | Multi-Spectral Video Camera | 18-110mm Zoom | - | Color-VTR 1" | 60 min | 30 fps | Width 39° - 7° | |
| 44 | Video System Monitor | - | - | B/W-VTR 1/2" | - | 30 fps | - | |

ADDITIONAL INFORMATION: * Tivicon - Texas Instruments electron scanned silicon-diode-array image tube spectral response 0.35 to 1.1 μ ; with W88A filter 0.74 to 1.1 μ

CONFIDENTIAL

SECRET

APPENDIX B

Data Record Summaries (U)

(U) Appendix B contains a review and comment for each useful data record obtained during Operation Dial Flower. These record commentaries have been separated by event and are arranged in the same order as the cameras appear in the relevant instrument plan (Appendix A). The final two digits of the record number correspond to the position numbers of cameras on the instrument plan and may be used to identify the camera employed for a particular record. The (P) and (N) nomenclature listed in the film type column denotes positive and negative type films respectively. Within the summary comments, "duration" indicates the maximum time after time zero that data was recorded.

SECRET

TABLE P-I (S)
TECHNOLOGY INTERNATIONAL CORPORATION
DATA RECORD SUMMARY (U)

OPERATION: Dial Flower DATE: 25 June 1972 STATION: USNS WHEELING
EVENT: Fr 44 LOCATION: OPAREA PROJ. ENGINEER: Deuel

| RECORD NO. | FILM TYPE | RECORD SUMMARY |
|------------|-------------------------|---|
| 61011 | Kodachrome II (P) | Good exposure; color cine record; general documentary coverage; wide angle; duration - 2 minutes |
| 61012 | Kodachrome II (P) | Good exposure; color cine record with azimuth reference; fireball evolution and transition to cloud; medium telephoto; duration - 1 minute |
| 61013 | Extended Range (XR) (N) | Good exposure; cine record defines fireball luminous cross-section; wide angle; duration - 30 seconds. |
| 61014 | High Speed Infrared (N) | Good exposure; infrared cine record with azimuth reference. fireball cross-section defined; wide angle, duration - 2 minutes |
| 61015 | Extended Range (XR) (N) | Good exposure; high speed cine record, fireball history and luminous cross-section defined throughout; medium angle, duration - 10 seconds |
| 61016 | Plus-X (N) | Good exposure; cine record in black/white for brightness history; shows luminous cross-section, fireball development, pre-zero balloon; medium angle; duration - 1 minute |
| 61017 | Kodachrome II (P) | Good exposure; highest spatial resolution cine record for late fireball and transition phase; telephoto, duration - 30 seconds |

SECRET

TABLE B-I continued (S)
TECHNOLOGY INTERNATIONAL CORPORATION
DATA RECORD SUMMARY (U)

OPERATION: Dial Flower DATE: 25 June 1972 STATION: USNS WHEELING
 EVENT: Fr 44 LOCATION: OPAREA PROJ. ENGINEER: Deuel

| RECORD NO. | FILM TYPE | RECORD SUMMARY |
|------------|--------------------------|---|
| 61021 | Ektachrome MS (P) | Good exposure; clock reference for 61022 and 61023, azimuth reference, shows general cloud cover; rate 1 frame/2 seconds early to 1 frame/30 seconds late times; duration - 40 minutes |
| 61022 | Ektachrome MS (P) | Good exposure; general debris cloud development; lower edge of debris cloud distinguishable for several minutes after top is obscured by natural clouds; rate and duration as for 61021. |
| 61023 | Infrared Aerographic (N) | Good exposure; debris cloud appears lighter than background (on negative) in infrared; rate and duration as for 61021. |
| 61024 | Ektachrome MS (P) | Dark exposure; good detail of fireball structure and debris cloud to H + 5 minutes. Lower edge distinguishable as on 61022; rate - 1 frame/second early time (luminous phase) with some late time data. |
| 61025 | Ektachrome MS (P) | Good exposure; high resolution of fireball and cloud development with short-lived stem and debris cloud-puff (left side). Shows pre-zero balloon; rate and duration as for 61024. |

SECRET

TABLE B-I continued (S)
TECHNOLOGY INTERNATIONAL CORPORATION
DATA RECORD SUMMARY (U)

OPERATION: Dial Flower DATE: 25 June 1972 STATION: USNS WHEELING
EVENT: Fr 44 LOCATION: OPAREA PROJ. ENGINEER: Deuel

| RECORD NO. | FILM TYPE | RECORD SUMMARY |
|------------|--------------------------|---|
| 61031 | Aerochrome Infrared (P) | Good exposure; clock and azimuth reference for 61032 and 61033; rate 1 frame/2 seconds early time to 1 frame/30 seconds late time; duration - 40 minutes. |
| 61032 | Ektachrome MS (P) | Good exposure; general cloud cover; lower edge of cloud visible to several minutes after general obscuration by natural clouds; rate and duration as for 61031. |
| 61033 | Infrared Aerographic (N) | Light exposure; general cloud cover; rate and duration as for 61031. |
| 61041 | Video Tape (1") | Good video record; visible light, wide angle; duration - 40 minutes. |
| 61042 | Video Tape (1/2") | Good video record; infrared filter, telephoto; pre-zero balloon visible; duration - 40 minutes. |
| 61043 | Video Tape (1") | Good video record; three color, wide angle, ND filter (variable); duration - 40 minutes. |
| 61044 | Video Tape (1/2") | Good video record; duration - 40 minutes. |

SECRET

SECRET

TABLE B-I continued (S)
TECHNOLOGY INTERNATIONAL CORPORATION
DATA RECORD SUMMARY (U)

OPERATION: Dial Flower DATE: 30 June 1972 STATION: USNS WHEELING
EVENT: Fr 45 LOCATION: OPAREA PROJ. ENGINEER: Deuel

| RECORD NO. | FILM TYPE | RECORD SUMMARY |
|------------|-------------------------|---|
| 61111 | Kodachrome II (P) | Good exposure; cine record; general documentary coverage; wide angle, duration - 2 minutes. |
| 61112 | Kodachrome II (P) | Dark exposure; cine record; late fireball development, shock wave condensation and near surface disturbance deflected medium telephoto duration - 1 minute. |
| 61113 | Extended Range (XR)(N) | Good exposure; azimuth reference; multi-image blurring; wide angle; duration - 30 seconds. |
| 61114 | High Speed Infrared (N) | Good exposure; cine record; fireball luminous cross-section defined; wide angle; duration - 2 minutes. |
| 61116 | Plus-X (N) | Good exposure; cine record; shows fireball evolution, pronounced shock wave condensation and brightness history; medium angle; duration - 1 minute. |
| 61117 | Kodachrome II (P) | Good exposure; cine record of late fireball development; telephoto; duration - 30 seconds. |

SECRET

TABLE B-I continued (S)
TECHNOLOGY INTERNATIONAL CORPORATION
DATA RECORD SUMMARY (U)

OPERATION: Dial Flower DATE: 30 June 1972 STATION: USNS WHEELING
 EVENT: Fr 45 LOCATION: OPAREA PROJ. ENGINEER: Devel

| RECORD NO. | FILM TYPE | RECORD SUMMARY |
|------------|--------------------------|--|
| 61121 | Ektachrome MS (P) | Good exposure; clock and azimuth reference for 61122 and 61123; shows fireball, and shock wave condensation, debris toroid development; rate - 1 frame 2 seconds early time to 1 frame/30 seconds late time; duration - 45 minutes. |
| 61122 | Ektachrome MS (P) | Good exposure; shows fireball, shock induced condensation, time history of debris toroid development including water vapor dissipation and left edge puff. Late time dispersed cloud visible to right side of field-of-view; rate and duration as for 61121. |
| 61123 | Infrared Aerographic (N) | Good exposure; shows natural cloud cover. rate and duration as for 61121. |
| 61124 | Ektachrome MS (P) | Dark exposure; medium resolution of fireball structure, debris toroid and dissipation of condensation; rate - 1 frame/second early time (luminous phase) with some late time data. |
| 61125 | Ektachrome MS (P) | Good exposure; high resolution of fireball, shock associated surface disturbance, support cable vapor, water column, and stem; rate and duration as for 61124. |

SECRET

TABLE B-I continued (S)
TECHNOLOGY INTERNATIONAL CORPORATION
DATA RECORD SUMMARY (U)

OPERATION: Dial Flower DATE: 30 June 1972 STATION: USNS WHEELING
EVENT: Fr 45 LOCATION: OPAREA PROJ. ENGINEER: Deuel

| RECORD NO. | FILM TYPE | RECORD SUMMARY |
|------------|--------------------------|---|
| 61131 | Aerochrome Infrared (P) | Good exposure; clock and azimuth reference for 61132 and 61133; rate - 1 frame/2 seconds early time to 1 frame/30 seconds late time; duration - 45 minutes. |
| 61132 | Ektachrome MS (P) | Dark exposure; shows fireball and shock induced condensation plus general cloud cover; rate and duration as for 61131. |
| 61133 | Infrared Aerographic (N) | Light exposure; fireball in six frames; rate and duration as for 61131. |
| 61141 | Video Tape (1") | Good video record; wide angle; duration - 45 minutes. |
| 61142 | Video Tape (1/2") | Good video record; infrared filter; telephoto; duration - 45 minutes. |
| 61143 | Video Tape (1") | Good video record; three color; telephoto; ND filter (variable); fireball well defined throughout; shows shock progression down cable vapors, shock induced disturbance on right side; duration - 45 minutes. |
| 61144 | Video Tape (1/2") | Good video record; duration - 45 minutes. |

SECRET

SECRET

TABLE B-1 continued (S)
TECHNOLOGY INTERNATIONAL CORPORATION
DATA RECORD SUMMARY (U)

OPERATION: Dial Flower DATE: 27 July 1972 STATION: USNS WHEELING
EVENT: Fr 46 LOCATION: OPAREA PROJ. ENGINEER: Deuel

| RECORD NO. | FILM TYPE | RECORD SUMMARY |
|------------|-------------------------|---|
| 61212 | Kodachrome II (P) | Dark exposure (filtered) defines fireball and heavy shock induced condensation escort ship in field-of-view; medium telephoto; duration - 1 minute. |
| 61213 | Kodachrome II (P) | Very dark exposure (filtered) shows some detail of fireball through dense shock induced condensation including luminous cross-section; wide angle; duration - 30 seconds. |
| 61215 | Extended Range (XR) (N) | Good exposure; highest speed cine record; fireball size defined at early times; medium angle, duration - 10 seconds. |
| 61216 | Plus-X (N) | Good exposure, cine record; defines fireball development and brightness history; medium angle; duration - 1 minute. |

SECRET

SECRET

TABLE B-I continued (S)
TECHNOLOGY INTERNATIONAL CORPORATION
DATA RECORD SUMMARY (U)

OPERATION: Dial Flower DATE: 27 July 1972 STATION: USNS WHEELING
EVENT: Fr 46 LOCATION: OPAREA PROJ. ENGINEER: Deuel

| RECORD NO. | FILM TYPE | RECORD SUMMARY |
|------------|--------------------------|--|
| 61221 | Ektachrome MS (P) | Good exposure; clock reference for 61222 and 61223, shows general cloud cover, ships in area (at least 4); rate - 1 frame/2 seconds early time to 1 frame/30 seconds late time; duration - 50 minutes. |
| 61222 | ACN-Color Negative (N) | Good exposure; for direct generation of positive prints as required; rate and duration as for 61221. |
| 61223 | Infrared Aerographic (N) | Good exposure; general coverage of area; rate and duration as for 61221. |
| 61224 | Ektachrome MS (P) | Good exposure; azimuth reference; luminous phase gives evidence of shower activity; shows dense shock wave condensation, surface stem, and debris induced veil over cap; good resolution of late debris torus and dissipation of condensation cloud although partially obscured by natural clouds; some late time debris; rate - 1 frame/second early time (luminous phase). |
| 61225 | Ektachrome MS (P) | Good exposure; shows ships in vicinity (including DeGrasse), high resolution fireball, stem near surface, debris cloud rising through break in clouds, and late debris torus including dispersal; rate and duration as for 61224. |

SECRET

SECRET

TABLE B-1 continued (S)
TECHNOLOGY INTERNATIONAL CORPORATION
DATA RECORD SUMMARY (U)

OPERATION: Dial Flower DATE: 27 July 1972 STATION: USNS WHEELING
EVENT: Fr 46 LOCATION: OPAREA PROJ. ENGINEER: Deuel

| RECORD NO. | FILM TYPE | RECORD SUMMARY |
|------------|--------------------------|--|
| 61231 | Aerochrome Infrared (P) | Light exposure; clock reference for 61232 and 61233; rate - 1 frame/2 seconds early time to 1 frame/30 seconds late time; duration - 50 minutes. |
| 61232 | Ektachrome MS (P) | Dark exposure; shows fireball development, general evolution and cloud cover in area; rate and duration as for 61231. |
| 61233 | Infrared Aerographic (N) | Light exposure; general coverage; rate and duration as for 61231. |
| 61241 | Video Tape (1") | Good video record; wide angle duration - 50 minutes. |
| 61242 | Video Tape (1/2") | Good video record; infrared filter; telephoto angle; pre-zero balloon visible at times but not immediately before zero; duration - 50 minutes. |
| 61243 | Video Tape (1") | Good video record; three color; telephoto angle, ND filter (variable); duration - 50 minutes. |
| 61244 | Video Tape (1/2") | Good video record; duration - 50 minutes. |

SECRET

SECRET

TABLE B-1 continued (S)
TECHNOLOGY INTERNATIONAL CORPORATION
DATA RECORD SUMMARY (U)

OPERATION: Dial Flower DATE: 31 July 1972 STATION: USNS WHEELING
EVENT: High Explosive Safety Experiment LOCATION: OPAREA PROJ. ENGINEER: Deuel

| RECORD NO. | FILM TYPE | RECORD SUMMARY |
|------------|-------------------------|--|
| 61311 | Kodachrome II (P) | Light exposure; cine record; wide angle; duration - 2 minutes. |
| 61312 | Kodachrome II (P) | Good exposure; azimuth reference; cine record shows flash below horizon and development of cloud; medium telephoto, duration - 1 minute. |
| 61313 | Kodachrome II (P) | Good exposure; cine record; wide angle; duration - 30 seconds. |
| 61315 | XR (extended range) (N) | Good exposure; high speed cine record; medium angle, duration - 10 seconds. |
| 61317 | XR (extended range) (N) | Good exposure; cine record of cloud development; telephoto, duration - 30 seconds. |

SECRET

SECRET

TABLE B-I continued (S)
TECHNOLOGY INTERNATIONAL CORPORATION

DATA RECORD SUMMARY (U)

OPERATION: Dial Flower DATE: 31 July 1972 STATION: USNS WHEELING
EVENT: High Explosive Safety Experiment LOCATION: OPAREA PROJ. ENGINEER: Deuel

| RECORD NO. | FILM TYPE | RECORD SUMMARY |
|------------|--------------------------|---|
| 61321 | Ektachrome MS (P) | Good exposure; clock and azimuth reference for 61322 and 61323; rate - 1 frame/2 seconds early time to 1 frame/30 seconds late time; duration - 20 minutes. |
| 61322 | ACN-Color Negative (N) | Good exposure; for direct generation of positive prints; rate and duration as for 61321. |
| 61323 | Infrared Aerographic (N) | Good exposure; shows development of cloud and drift; rate and duration as for 61321. |
| 61324 | Ektachrome MS (P) | Good exposure; high resolution includes zero flash below horizon, cloud development and dispersion; azimuth reference; rate - 1 frame/second early time with some late time data. |
| 61325 | Ektachrome MS (P) | Good exposure; close approach of DeGrasse before zero; high resolution of zero flash below horizon; rate as for 61324. |

SECRET

TABLE B-1 continued (S)
TECHNOLOGY INTERNATIONAL CORPORATION
DATA RECORD SUMMARY (U)

OPERATION: Dial Flower DATE: 31 July 1972 STATION: USNS WHEELING
 EVENT: High Explosive Safety Experiment LOCATION: OPAREA PROJ. ENGINEER: Deuel

| RECORD NO. | FILM TYPE | RECORD SUMMARY |
|------------|--------------------------|---|
| 61331 | Aerochrome Infrared (P) | Good exposure; clock and azimuth reference for 61332 and 61333, shows general cloud motion and structure; rate - 1 frame/2 seconds early time to 1 frame/30 seconds late time; duration - 20 minutes. |
| 61332 | Ektachrome MS (P) | Good exposure; shows azimuth reference, zero flash below horizon, development and drift of cloud; rate and duration as for 61331. |
| 61333 | Infrared Acrographic (N) | Light exposure; rate and duration as for 61331. |
| 61341 | Video Tape (1") | Good video record; wide angle; duration - 20 minutes. |
| 61342 | Video Tape (1/2") | Good video record; infrared filter, telephoto; duration - 20 minutes. |
| 61343 | Video Tape (1") | Good video record; three color; narrow angle, ND filter (variable) duration - 20 minutes. |
| 61344 | Video Tape (1/2") | Good video record; duration - 20 minutes. |

UNCLASSIFIED

APPENDIX C

REFRACTIVE CORRECTION (U)

(U) When considering sources of discrepancies in optical measurements dealing with the geometry of varied atmospheric phenomenon, an investigation must be made of the effects of refraction. Many tables have been compiled for use in astronomy and navigation which list refractive corrections for zenith angle measurements on stars viewed through all of the atmosphere. Apparently little information, however, is published concerning the magnitude of the refractive correction necessary for accurate altitude measurements within the atmosphere. It is this type of correction which must be applied to target altitude for the particular case in which we are interested.

(U) The effect of refraction is to bend the light rays downwards causing the observer to perceive a target altitude higher than its true geometrical position. Thus reference to Figure C-1 will show that though the actual altitude of the target is T, it appears to be at A along a line tangent to the curving ray at the location of the observer. Therefore, the correction AT must be calculated to determine actual target altitude.

(U) Information is available concerning the radius of curvature, R, of a light ray within the atmosphere (Ref. 7). This radius as a function of temperature, pressure, and lapse rate, is given by:

$$R = \frac{1.266 \times 10^4 T^2}{P(34 - \Gamma)} \quad (C-1)$$

where

P is atmospheric pressure in millibars

T is temperature in °K

Γ is the negative of temp change with height
in °K/km (lapse rate)

UNCLASSIFIED

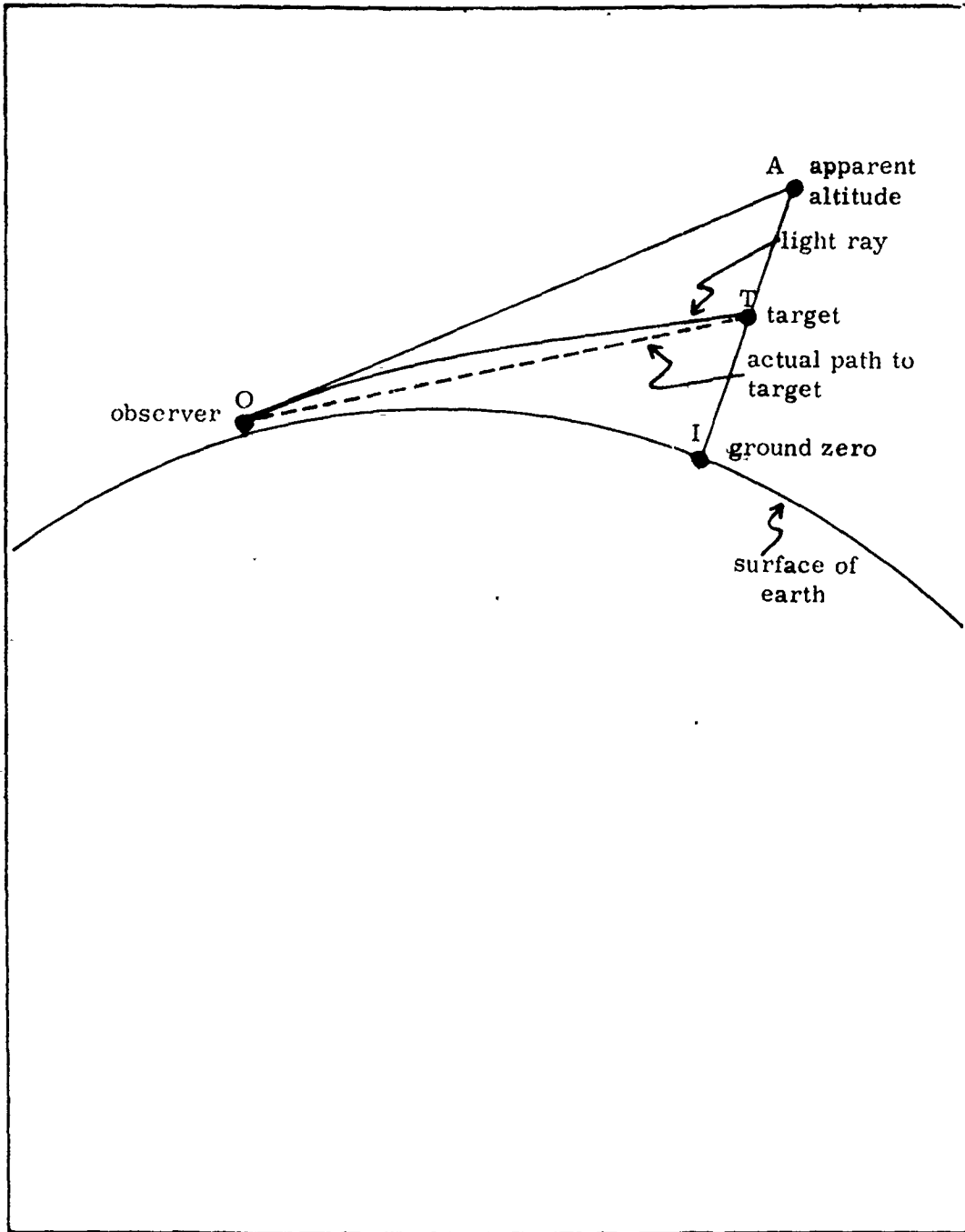


Figure C-1 (U). Geometrical model for terrestrial refraction calculation (U).

UNCLASSIFIED

UNCLASSIFIED

(U) In order to calculate the vertical distance at the target between the curving light path and the tangent, simple geometry configurations are used. Figure C-2 shows the configuration with the separation between the curve and the tangent being given by:

$$s = R (\sec \alpha - 1) \quad (C-2)$$

the value of α in radians is:

$$\alpha = \frac{OT}{R}$$

(U) In the case being considered the distance OT can be approximated by the known distance from the observer to ground zero, OI. The error in the calculation of α introduced by this approximation is less than .01%. Equation (C-2) then becomes

$$s = R \left[\sec \frac{OI}{R} - 1 \right] \quad (C-3)$$

(U) As the atmospheric conditions change with altitude so must the radius of curvature. Using atmospheric temperature and pressure information from reference 4 to solve for the radius of curvature, the resulting separation can be determined from equation (C-3). Table C-1 gives the separations for various altitudes assuming the light is subject to the conditions of one altitude for its entire path. Over 20 nm the separation would be 18.15 meters for a path at sea level conditions and 12.29 meters for a path at 5000 meters. Therefore, a path extending from sea level to an altitude of 5000 meters would have a refractive correction between 18 and 12 meters.

(U) In order to get a better approximation, the atmosphere can be divided into 500 meter thick layers in which the amount of refraction occurring in each layer is calculated. Summing each layer, the total amount of refraction is found. Flat layers of air density can be assumed since over 20nm the earth's curvature is relatively flat. Thus the amount

UNCLASSIFIED

of refraction occurring in a layer is proportional to the amount of total path which is situated in that layer. Table C-2 illustrates the resulting calculation of refractive correction for a path extending from sea level to a 5000 meter altitude.

(U) Thus the refractive correction for the 0 - 5000 m path is 15.1 meters or 3% of the original height. For a target altitude of 500 meters, the correction is 18.1 meters or 4% of the observed height. Though many approximations are used to calculate the refractive correction, the error bar on these calculations is estimated to be no more than 5% (~ 1 meter).

UNCLASSIFIED

TABLE C-1 (U)

LIGHT PATH RADIUS OF CURVATURE AS A FUNCTION OF ALTITUDE (U)

| Altitude, (meters) | Radius of Curvature, (km) | Separation,* (meters) |
|-----------------------|------------------------------|--------------------------|
| 0 | 37,719 | 18.15 |
| 1,000 | 40,627 | 16.85 |
| 2,000 | 43,834 | 15.62 |
| 3,000 | 47,380 | 14.45 |
| 4,000 | 51,308 | 13.34 |
| 5,000 | 55,672 | 12.29 |
| 6,000 | 60,532 | 11.31 |
| 7,000 | 65,960 | 10.38 |
| 8,000 | 72,040 | 9.50 |
| 9,000 | 78,873 | 8.68 |
| 10,000 | 86,574 | 7.90 |
| 12,000 | 111,370 | 6.15 |
| 14,000 | 152,467 | 4.49 |
| 16,000 | 208,689 | 3.28 |
| 18,000 | 285,585 | 2.40 |
| 20,000 | 390,739 | 1.75 |

*Difference between actual and tangent to light path (ref. Fig. C-1) for given altitude conditions.

TABLE C-2 (U). DETERMINATION OF REFRACTION ALONG SLANT PATH (U)

| Altitude, (m) | Radius Curvature, (km) | Refraction for 20nm In Conditions of Layer, (m) | Fraction of Total Path in Layer | Refraction in Layer, (m) |
|--------------------|---------------------------|--|------------------------------------|-----------------------------|
| 0 - 500 | 37,719 | 18.15 | .1 | 1.82 |
| 500 - 1500 | 40,627 | 16.85 | .2 | 3.37 |
| 1500 - 2500 | 43,834 | 15.62 | .2 | 3.12 |
| 2500 - 3500 | 47,380 | 14.45 | .2 | 2.89 |
| 3500 - 4500 | 51,308 | 13.34 | .2 | 2.67 |
| 4500 - 5000 | 55,672 | 12.29 | .1 | 1.23 |
| TOTAL REFRACTION - | | | | 15.10 meters |

UNCLASSIFIED

APPENDIX D

ATMOSPHERIC TRANSMISSION (U)

(U) The method of determining the transmittance of the atmosphere between the platform and the event in the four colorbands used in the radiometric analysis section is complicated by a lack of knowledge of the precise composition of the atmosphere on that day. Transmittance is reduced by the processes of scattering and absorption along the path of the light ray from source to detector. The amount of scattering and absorption is dependent on the amount and type of material composing the transmitting medium.

(U) The transmittance through a given thickness of a homogeneous substance of uniform density can be expressed as a simple exponential. In terms of the notation used in section 5.4.2,

$$T(\lambda) = e^{-\int \alpha(r, \lambda) dr} \quad (D-1)$$

where T is the transmittance; r is the distance through the medium which the light must travel, and $\alpha(\lambda)$ is the combined scattering and absorption cross section per unit volume of material including all the constituents of the atmosphere in question.

(U) The integral $\int \alpha(\lambda) dr$, referred to as the optical depth, is in this discussion designated by $\rho(\lambda)$. The optical depth, a dimensionless quantity, is a measure of the attenuation experienced by a certain wavelength of light over a given path in a medium of a given composition, distribution, and physical state.

(U) For a sea-level path over the ocean, this integral can be simplified and reduced to:

$$\rho(\lambda) = r \sum_i n_i [\sigma_i + \kappa_i] \quad (D-2)$$

UNCLASSIFIED

(U)

where n_i is the concentration of the i th component of the atmosphere, σ_i is the scattering cross section of the i th component, and κ_i is the absorption cross section of the i th component.

(U) In this particular case, three atmospheric components need to be considered: molecular gases, water vapor, and aerosols. These components contribute in several ways to the attenuation of visible light via molecular scattering, σ_m , water vapor absorption, κ_{H_2O} , aerosol scattering, σ_a , and aerosol absorption, κ_a . The contribution of each of these is discussed and the optical depth and transmissions are then calculated according to equation (D-1) and (D-2) above. For these calculations, a range of 35.7 kilometers (20 nautical miles) was assumed. On the day of the event, the temperature at the ship was measured at 25°C and the humidity at 74%. Although there was a 19-knot wind, the sea was relatively calm and the sky appeared clear between the ship and the event.

Aerosols (U)

(U) In the IR region, aerosol scattering is the dominant source of atmospheric attenuation. Aerosols range from roughly $10^2 \mu$ to $10^{-3} \mu$ in diameter. They are grouped in three size categories: giant particles from 100 to 1 μ in diameter, large particles from 1 to .1 μ , and Aitken particles from .1 to .001 μ . The large particles are primarily responsible for optical haze. Reference 5 gives scattering and absorption cross sections for two models of aerosol concentrations corresponding to "clear" and "hazy" conditions. Clear conditions are considered to be a visibility of 23km, and hazy conditions a visibility of 5km. Since the event was 36km distant and plainly visible, one might expect the actual aerosol concentration to be less than the minimum necessary for 23km visibility. The main aerosol contribution is assumed to be dust and the data supplied refers to continental air. As the

UNCLASSIFIED

UNCLASSIFIED

(U)
event took place over the ocean, questions about the nature and quantity of the aerosol content must be considered.

(U) In Figures 5 - 25 and 5 - 26 of reference 4, the size distribution functions of aerosols in continental and maritime air are given along with techniques for integration to determine the number of particles in a given size regime. On the assumption that the optical thickness in the visible and near-infrared regions is proportional to the number of large particles, the distribution curves were integrated to find the total number of large particles in continental and maritime air. The ratios of the absorption and scattering cross sections of aerosols in maritime air to continental air were assumed to be equal to the ratio of the number of large particles in these respective environments. This particle ratio, determined to be .055 with an uncertainty factor of two, was then used to calculate aerosol cross-sections for maritime air from the cross-sections for clear continental air. The cross sections were derived for a unit horizontal path length of one kilometer.

Water Vapor (U)

(U) For the event day conditions of 25^o C temperature and 74% humidity, Figure 10-3 of reference 4 gives the number of precipitable centimeters of water vapor in a horizontal path length as 1.7cm/km. Allen (reference 6) gives the water vapor absorption cross section as a function of wavelength in terms of precipitable centimeters per unit path length. For example at $\lambda = 800\text{nm}$, the water vapor absorption cross section is given as .001/precipitable cm. Then for event day conditions:

$$\kappa_{\text{H}_2\text{O}} = .001/\text{cm} \times 1.7\text{cm}/\text{km} = .0017/\text{km}$$

UNCLASSIFIED

Molecular (U)

(U) Molecular scattering coefficients per kilometer horizontal path length were taken from graphs found in reference 5.

Results (U)

(U) The cross sections obtained at each wave length were added together and multiplied by the range (35.7 km) to determine the optical depth. The transmittance for each wavelength was then determined by equation (D-1). The results of these calculations are summarized in Table D-1.

UNCLASSIFIED

TABLE D-1. (U) ATMOSPHERIC PROPERTIES (U)

Temperature = 25° C; Humidity 74%; Wind = 19 knots

Aerosols:

| λ | σ_a^* | κ_a^* | .055 σ_a | .055 κ_a |
|-----------|--------------|--------------|-----------------|-----------------|
| 4200 | .157 | 0 | .0086 | 0 |
| 5500 | .134 | 0 | .0074 | 0 |
| 6500 | .117 | .014 | .0064 | .0008 |
| 8100 | .105 | .0105 | .0058 | .0006 |

Water Vapor:

| λ | κ per cm |
|-----------|-----------------|
| 4200 | .0036 |
| 5500 | .002 |
| 6500 | .002 |
| 8100 | .001 |

Total Cross Sections:

Range = 35.7 km

| λ | σ_a | κ_a | σ_m | κ_{H_2O} | Total | ρ | τ_a |
|-----------|------------|------------|------------|-----------------|-------|--------|----------|
| 4200 | .0086 | - | .038 | .006 | .0526 | 1.88 | .15 |
| 5500 | .0074 | - | .011 | .003 | .0214 | .76 | .47 |
| 6500 | .0064 | .0008 | .0055 | .003 | .0157 | .56 | .57 |
| 8100 | .0058 | .0006 | .002 | .002 | .0100 | .37 | .69 |

*23 km visibility model from reference 5.

UNCLASSIFIED

SECRET

DISTRIBUTION LIST

This document is being sent to the below listed contractors for the use of the individuals listed. Recipient contractors are requested to validate individuals' clearances before forwarding document to same.

DEPARTMENT OF DEFENSE

Defense Documentation Center
Cameron Station
2 cy ATTN: TC

Director
Defense Nuclear Agency
ATTN: STSI
ATTN: STTL
2 cy ATTN: RAAE

DEPARTMENT OF THE NAVY

Director
Ballistic Missile Defense Advanced Tech Center
ATTN: H. Porter

Director
Ballistic Missile Defense Prog. Office
ATTN: J. Shea

Commander
Naval Surface Weapons Center
ATTN: Code 213, W. Derken

DEPARTMENT OF THE AIR FORCE

AF Cambridge Research Labs. AFSC
ATTN: OPR, H. Gauvin

AF Weapons Laboratory, AFSC
ATTN: DYT, D. Matuska

AFTAG
ATTN: TF, R. Wiley

ATOMIC ENERGY COMMISSION

Los Alamos Scientific Laboratory
2 cy ATTN: Document Control for M. Peek

DEPARTMENT OF DEFENSE CONTRACTORS

Aerospace Corporation
ATTN: D. Rawcliffe

General Electric Company
TEMPO-Center for Advanced Studies
ATTN: T. Barret
2 cy ATTN: DASIAC

General Research Corporation
ATTN: J. Ise

HSS, Inc
ATTN: D. Hansen

DEPARTMENT OF DEFENSE CONTRACTORS (Continued)

Institute for Defense Analyses
ATTN: H. Wolfhard

Lockheed Missiles and Space Company, Inc
ATTN: LMSCPA for J. Kumer

Mission Research Corporation
ATTN: D. Sappenfield

R & D Associates
ATTN: R. Lelevier

Stanford Research Institute
ATTN: W. Chesnut

Technology International Corporation
ATTN: W. Boquist

UNCLASSIFIED

SECRET



DEFENSE THREAT REDUCTION AGENCY
Defense Threat Reduction Information Analysis Center (DTRIAC)
1680 TEXAS STREET SE
KIRTLAND AFB, NM 87117-5669

OP-CSUI (505) 853-0644

12 May 2009

To: DTIC-OQ

Subject: Distribution Review

DTRA has reviewed the following declassified documents and assigned Distribution Statement A, per FOIA Review, 28 April 2009:

ADC950035
Operation Dial Flower Analysis of High Resolution Optical Data (U)
26 November 1974. DNA 3396F

ADC950036
Optical Measurements for Operational Hula Hoop (U)
26 November 1974. DNA 3395F

ADC950196
High Resolution Optical Measurements for DNA Operation
Dice Game – Field Report (U)
16 July 1975. DNA 3670F

ADC950226
Data Analysis of High Resolution Photographic Records from DNA
Operation Hula Hoop-1973 (U)
May 1975. DNA 3714F

for 
Steven Bradford
Program Manager,
Defense Threat Reduction Information
Analysis Center (DTRIAC)